
AFRL-RW-EG-TP-2011-006

# PROJECT SUMMARY: BIOLOGY-INSPIRED AUTONOMOUS CONTROL

Johnny H. Evers

Air Force Research Laboratory, Munitions Directorate
AFRl/RWAV
101 West Eglin Blvd,
Eglin AFB, FL 32542

February 2011

INTERIM REPORT



**AIR FORCE RESEARCH LABORATORY**
**MUNITIONS DIRECTORATE**

■ **Air Force Materiel Command** ■ **United States Air Force** ■ **Eglin Air Force Base, FL 32542**

# REPORT DOCUMENTATION PAGE

*Form Approved*
*OMB No. 0704-0188*



| 1. REPORT DATE | 2. REPORT TYPE | 3. DATES COVERED *(From - To)* |
|---|---|---|
| 02-2011 | Interim | Oct 09 – Feb 11 |

**4. TITLE AND SUBTITLE**

Project Summary: Biology-Inspired Autonomous Control

**5a. CONTRACT NUMBER**
N/A

**5b. GRANT NUMBER**
N/A

**5c. PROGRAM ELEMENT NUMBER**
61602FF

**6. AUTHOR(S)**

Johnny H. Evers

**5d. PROJECT NUMBER**
2304

**5e. TASK NUMBER**
AM

**5f. WORK UNIT NUMBER**
08

**7. PERFORMING ORGANIZATION NAME(S) AND ADDRESS(ES)**
Air Force Research Laboratory, Munitions Directorate
AFRL/RWAV
101 West Eglin Blvd
Eglin AFB, FL 32542-6810

**8. PERFORMING ORGANIZATION REPORT NUMBER**

AFRL-RW-EG-TP-2011-006

**9. SPONSORING / MONITORING AGENCY NAME(S) AND ADDRESS(ES)**
Air Force Research Laboratory, Munitions Directorate
AFRL/RWAV
101 West Eglin Boulevard
Eglin AFB, FL 32542-6810

**10. SPONSOR/MONITOR'S ACRONYM(S)**
AFRL-RW-EG

**11. SPONSOR/MONITOR'S REPORT NUMBER(S)**
SAME AS BLOCK 8

**12. DISTRIBUTION / AVAILABILITY STATEMENT**

**DISTRIBUTION A:** Approved for public release; distribution unlimited. 96 ABW/PA Approval and Clearance # 96 ABW-2011-0085, dated 17 February 2011.

**13. SUPPLEMENTARY NOTES**

**14. ABSTRACT**

The goal of this project is to motivate development of control concepts for autonomous munitions that overcome limitations of conventional approaches by applying principles derived from studying the biology of flying organisms. The research is focused on understanding the mechanisms of biological flight through collaboration with various experimental biology academic research laboratories around the world. This exploration of biological flight includes behavior, vision and other sensory systems, flapping flight mechanics and aerodynamics, and flight control. The research focus addresses two broad, interrelated research areas: concepts for aeroelastic, propulsive flight inspired by the biomechanics, aerodynamics, sensing and neurobiology of flapping flight and wide field sensory-response inspired by the behavior and neurobiology of associated with spatial orientation, target pursuit and navigation in insects, birds and bats. With insight from these biology studies, the research seeks to motivate and develop new guidance and control concepts, theory, and methods for advanced munitions and micro air vehicle programs.

**15. SUBJECT TERMS**
Aeroelastic propulsive flight, wide field sensory-response, autonomous flight

| 16. SECURITY CLASSIFICATION OF: | | | 17. LIMITATION OF ABSTRACT | 18. NUMBER OF PAGES | 19a. NAME OF RESPONSIBLE PERSON |
|---|---|---|---|---|---|
| a. REPORT | b. ABSTRACT | c. THIS PAGE | | | Johnny Evers |
| UNCLASSIFIED | UNCLASSIFIED | UNCLASSIFIED | UL | 46 | 19b. TELEPHONE NUMBER *(include area code)* 850-883-1887 |

**CONTENTS**

BIOLOGY-INSPIRED AUTONOMOUS CONTROL



R. A. Thompson, J. H. Evers, K. C. Stewart, “Attitude Control Augmentation Using Wing Load Sensing – A Biologically Motivated Strategy”, 2010 AIAA Guidance, Navigation and Control Conference.

Z. E. Fuchs, P. P. Khargonekar, J. Evers, “Cooperative Defense within a Single-Pursuer, Two-Evader Pursuit Evasion Differential Game”, 2010 IEEE Conference on Decision and Control.

A. Chakravarthy, R. Albertani, J. Evers, “In-Flight Dynamically Adaptive Configurations: Lessons from Live Lepidoptera”, 2010 AIAA Adaptive Structures Conference.

A. Chakravarthy, K. A. Evans, J. Evers, “Sensitivities & Functional Gains for a Flexible Aircraft-Inspired Model”, 2010 American Control Conference.

J.H. Evers, “Issues of Scale in Agile Micro Autonomous Systems”, 2009 AIAA Unmanned…Unlimited Conference and Exhibit.

***PROJECT SUMMARY***

BIOLOGY-INSPIRED AUTONOMOUS CONTROL

AFOSR Laboratory Research Task 00MN02COR

Johnny Evers, Principal Investigator
Flight Vehicles Integration Branch, Munitions Directorate
Air Force Research Laboratory, Munitions Directorate
Eglin AFB, FL

**Abstract**
The goal of this project is to motivate development of control concepts for autonomous munitions that overcome limitations of conventional approaches by applying principles derived from studying the biology of flying organisms. The research is focused on understanding the mechanisms of biological flight through collaboration with various experimental biology academic research laboratories around the world. This exploration of biological flight includes behavior, vision and other sensory systems, flapping flight mechanics and aerodynamics, and flight control. The research focus addresses two broad, interrelated research areas: concepts for ***aeroelastic, propulsive flight*** inspired by the biomechanics, aerodynamics, sensing and neurobiology of flapping flight and ***wide field sensory-response*** inspired by the behavior and neurobiology of associated with spatial orientation, target pursuit and navigation in insects, birds and bats. With insight from these biology studies, the research seeks to motivate and develop new guidance and control concepts, theory, and methods for advanced munitions and micro air vehicle programs.

**Recent Progress**
Publications listed below highlight some of the research conducted under this project over the past two years. The first paper investigates the potential for load sensors on small air vehicle aerodynamic surfaces to enhance body platform stability. Two complementary techniques are explored: one using body torque error to control actuator position and the other using body force sensing to compensate for high optical feedback latency. The benefits of responding reflexively to forces on the aerodynamic surfaces include low latency, a reference frame inherently consistent with the control actuation, and alleviation of the necessity for control based explicitly on aerodynamic characterization. This paper uses 6DOF simulation to demonstrate the robustness derived from load sensing in a turbulent flow field with high levels of plant uncertainty and optical feedback latency. The results of this paper suggest that direct sensing of forces acting on the body can significantly enhance the robustness and performance of an attitude control system, perhaps giving insight into how natural systems can fly with high levels of damage, coarse sensors, and large sensorimotor information processing latencies.

The second paper is motivated by a desire to develop analytical formulations for cooperative defensive strategies against predator(s). A single-pursuer, two-evader differential game with a novel cost functional is formulated. Each of the three agents are modeled as mass less particles that move with constant velocity. The pursuer attempts to capture either of the evaders while minimizing its cost. Simultaneously, the evaders strive to maximize the pursuer's cost. The proposed cost functional represents the increased cost to the pursuer when presented with multiple, potentially dangerous targets. It captures the effect of cooperation between the evaders. In order to solve the game, optimality conditions for the equilibrium strategies are developed. The resulting system of ordinary differential equations is then integrate backwards in time from the terminal conditions to generate the optimal trajectories of the three agent system. The resulting trajectories display cooperative behaviors between the two evaders, which are qualitatively similar to behaviors found in predator-prey interactions in nature. A brief description of singular surfaces is also included.

The third paper discusses the collection, post-processing and subsequent evaluation of flight data of butterflies, in various free flight scenarios in a quasi-natural environment. A vision tracking system is used to obtain the flight data. This in turn is used to determine estimates of the motion of different body parts of the insect, including the abdomen and the wings. These estimates are subsequently analyzed with a view to establishing the manner in which the insect adapts the motion of its abdomen to work in tandem with the motion of its wings. Furthermore, the manner in which this adaptation changes through different flight phases is studied.

The fourth paper explores the issues of control of aeroelastic wing micro autonomous aerial systems. Controllers designed using methods applicable to larger aircraft are unlikely to realize the agile flight potential of flexible wing micro autonomous aerial systems airframes. In this paper, two Euler-Bernoulli beams connected to a rigid mass represent a conceptual model of an aeroelastic wing micro autonomous aerial system. Continuous Sensitivity Equation Methods are employed to examine the sensitivity of the controlled state with respect to variation of the $H_{Infinity}$ control parameter, with the primary goal being to gain insight into the flexible dynamics of the system in order to exploit the flexibility for control purposes. The paper further examines functional gains in order to determine optimal sensor placement while taking advantage of the flexibility of the micro autonomous aerial systems model.

The final paper of this collection addresses some of the technical challenges associated with development of bird or insect size micro autonomous aerial systems. It takes the perspective that agile micro autonomous aerial systems with their layers of human supervision represent complex, highly nonlinear multi-scale dynamical systems. After a brief discussion of some issues of scale for such systems and current research investigating those issues, the paper focuses on the idea of autonomy associated with multi-scale dynamical systems. Agile micro autonomous aerial systems currently exist only in nature (i.e., insects, birds, bats). Consequently, the paper considers autonomy in manmade micro autonomous aerial systems from a biological perspective. It introduces a conjecture that functional system characteristics associated with the capabilities of living flying organisms may require levels of response variation and flexibility that are not associated with, and perhaps will not be tolerated in manmade critical systems. Although this paper does directly address questions of ethics associated with the deployment of critical autonomous systems, it attempts to provide some insight into how those important questions may naturally emerge when any degree of robustness is imposed as a design criterion for manmade agile autonomous systems.

## PUBLICATIONS

R. A. Thompson, J. H. Evers, K. C. Stewart, “Attitude Control Augmentation Using Wing Load Sensing – A Biologically Motivated Strategy”, 2010 AIAA Guidance, Navigation and Control Conference.

Z. E. Fuchs, P. P. Khargonekar, J. Evers, “Cooperative Defense within a Single-Pursuer, Two-Evader Pursuit Evasion Differential Game”, 2010 IEEE Conference on Decision and Control.

A. Chakravarthy, R. Albertani, J. Evers, “In-Flight Dynamically Adaptive Configurations: Lessons from Live Lepidoptera”, 2010 AIAA Adaptive Structures Conference.

A. Chakravarthy, K. A. Evans, J. Evers, “Sensitivities & Functional Gains for a Flexible Aircraft-Inspired Model”, 2010 American Control Conference.

J.H. Evers, “Issues of Scale in Agile Micro Autonomous Systems”, 2009 AIAA Unmanned…Unlimited Conference and Exhibit.

# Attitude Control Augmentation Using Wing Load Sensing - A Biologically Motivated Strategy

Rhoe A. Thompson* Johnny H. Evers† Kelly C. Stewart‡
*AFRL/RW, Eglin AFB, FL, 32542, USA*

**Many flying animals are able to achieve highly robust flight without feedback from dedicated angular rate sensors. In general, these animals use their vision systems to provide attitude rate and orientation information. Limitations of vision based measurements for stabilizing the body include the high level of latency incurred in the visual processing system and the need to maintain some level of ocular isolation in order to achieve adequate image quality. This paper investigates the potential for load sensors on the aerodynamic surfaces to enhance body platform stability. Two complementary techniques are explored: one using body torque error to control actuator position and the other using body force sensing to compensate for high optical feedback latency. The benefits of responding reflexively to forces on the aerodynamic surfaces include low latency, a reference frame inherently consistent with the control actuation, and alleviation of the necessity for control based explicitly on aerodynamic characterization. This paper uses 6DOF simulation to demonstrate the robustness derived from load sensing in a turbulent flow field with high levels of plant uncertainty and optical feedback latency. The results of this paper suggest that direct sensing of forces acting on the body can significantly enhance the robustness and performance of an attitude control system, perhaps giving insight into how natural systems can fly with high levels of damage, coarse sensors, and large sensorimotor information processing latencies.**

## Nomenclature

| | | | |
|---|---|---|---|
| $\psi$ | Azimuth or Yaw Euler Angle | $\omega_n$ | Natural Frequency |
| $\theta$ | Elevation or Pitch Euler Angle | $J$ | Moment of Inertia |
| $\phi$ | Bank or Roll Euler Angle | $\zeta$ | Damping Ratio |
| $V$ | Inertial Velocity Magnitude | $K_p, K_d$ | Proportional and Derivative Control Gains |
| $[p, q, r]$ | Body Angular Rate Components | $K_t$ | Gain Associated with Torque Feedback |
| $b$ | Reference Lateral Length | $\Delta t_{opt}$ | Optical Feedback Latency |
| $c$ | Reference Longitudinal Length | $\theta_m, \dot{\theta}_m, T_m$ | Measured Angle and Torque States |
| $LQR$ | Linear Quadratic Regulator | $PD$ | Proportional Derivative Control |
| $MAV$ | Micro Air Vehicle | $PID$ | Proportional Integral Derivative Control |
| $6DOF$ | Six Degree of Freedom Simulation | $PDT$ | Proportional Derivative Torque Control |
| $GenMAV$ | Generic Micro Air Vehicle | | |

## I. Introduction

Insects are commonly used as research subjects for flight control physiology studies due to the reduced complexity of their morphology, physiology, and behavioral response. The ability of insects to perform precision navigation is also widely studied.[1,2] Flying insects are abundant and readily available, and they are considered models for the characteristics desired in man-made micro-air vehicles.[3,4] Insects robustly deal with damage to their bodies and uncertainty in their environments. They are adaptable, autonomous, and can readily change behavioral objectives. Insects, in all of their various forms, have a wide array of discrimination and target-tracking capabilities, using optical, acoustic and chemo-receptive modalities.[5,6,7] All flying insects appear to take advantage of optical rate feedback in their flight control systems. Insects of the order Diptera, flies, also use mechanoreceptive angular rate feedback from the halteres.[8,9,10] Those insects having only optical rate feedback are capable of remarkable flight performance. Given the amount of latency inherent in the optical feedback pathways, the specific mechanisms through which flight stability is

*rhoe.thompson@eglin.af.mil, AFRL/RWGG, AIAA Member
†johnny.evers@eglin.af.mil, AFRL/RWAV, AIAA Member
‡kelly.stewart@eglin.af.mil, AFRL/RWGN, AIAA Member

achieved remain unclear.[11] It is this characteristic that is the motivation for the work described in this paper.

The intent of this research is to understand the benefits of load sensing on aerodynamic surfaces for attitude stabilization. The bodies of animals are sensor rich. Strain sensors that respond to internal and external forces on the exoskeleton are common if not universal.[12,13] In addition to having influence on high-level behaviors, these sensors have evolved to provide low-latency reflexive response as well. The wings of insects have cuticular strain sensors, referred to as campaniform sensilla, distributed along the structural veins, as well as chordotonal organs that stretch and respond to motion of the wing hinge.[14] These sensors encode magnitude of the wing load through species-dependent mechanisms.[15] The pathways to the wing control muscles are short, with low latency, leading to speculation that they are directly involved in flight control.[16] Given the relatively high level of latency involved in rate feedback from the insect visual system, it is likely that the wing load sensors play a direct role in attitude stabilization. This role is especially indicated in natural systems that do not have a direct, low-latency means of measuring angular rate attached to the main body, i.e., halteres or other gyroscopic organs.

The point of departure for this activity was a subsequently discarded hypothesis: strain sensed on the wings is proportional to angular rate in the body frame. Therefore, by reacting to wing strain, a winged vehicle could apply a dissipative damping force that ensures attitude stability. The origin of this thought process was the understanding that a steady state roll motion would induce a differential angle of attack on the wings proportional to roll rate. This differential angle of attack would in turn result in a differential force, or roll damping, on the wings which might be sensed and controlled. Therefore, the differential wing load would be proportional to roll rate. While the described rate damping effects are very real, the inability to separate other dynamic causal effects, e.g., control surface deflection and transient gusts, from the steady state mechanism hypothesized was felt to be insurmountable. Alternative mechanisms were therefore pursued.

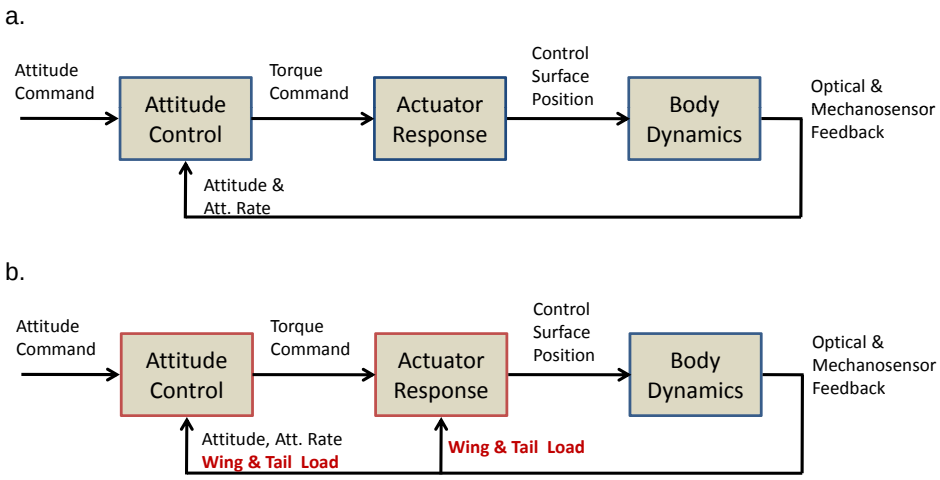


**Figure 1. a) Baseline attitude control without load feedback. Actuators assumed have a first order open-loop response. b) Attitude with load feedback to optimize responsiveness of the attitude controller and to reject disturbances and errors in actuated body torque. The closed-loop actuator response is modeled as a damped second order system.**

In its simplest form, the attitude control of a flight vehicle can be described as in Figure 1a. Angular rate and orientation resulting from the system dynamics are sensed, and the measurements are fed back into the attitude control system. The attitude control system then commands a control surface response, intended to produce a torque on the body in order to reduce attitude state errors. There are two fundamentally distinct ways in which strain measurements might influence the attitude control design: through regulation of the actuation commands sent to the control surfaces and through augmentation of the attitude controller, Figure 1b. In the first way, the measured error in the body torque achieved by the vehicle control surfaces can be driven to zero using the actuators. The source of this error might be uncertainty in the plant characteristics or a torque disturbance on the body from external sources such as turbulence. The second way that load sensing might be used in the control system, direct use in the attitude control formulation, has multiple possibilities as well. Attitude control systems normally include proportional and integral control on sensed attitude, with damping and robustness provided through rate feedback. A disturbance force acting on the body must produce body angular rate before the controller moves the control effectors to cancel it. If some direct measure of angular acceleration could be sensed, the attitude controller could potentially obtain a more optimal tracking response. In addition, if torque was estimated from the strains sensed, with knowledge of the inertia, a low latency measure of

angular acceleration could be obtained. With this estimate, high-latency optical angular rate feedback, or phase error, might be directly mitigated to a first order.

## II. Model and Simulation Description

**Figure 2. Attitude control demonstrations were based on a model of the AFRL GenMAV vehicle. Aerodynamic coefficients were calculated using AVL. Models assumed a configuration with ailerons, not shown in the hardware depicted.**

The specific mechanisms by which load sensing is used in natural systems for flight stabilization are not known. To demonstrate potential applications and the associated benefits, a model of the Air Force Research Laboratory (AFRL) developed Generic Micro-Air-Vehicle (GenMAV) was employed, as shown in Figure 2. This choice avoided the complexity of modeling a flapping wing system, allowing for more straightforward conceptualization of engineering applications, while still providing direct insight into potential biological mechanisms.

GenMAV is a conventionally-shaped air vehicle with a high-wing configuration, a wingspan of 24" and a chord of 5". It has a conventional tail with a horizontal surface of 12" and a vertical surface of 4.6". The fuselage is 16.5" in length and approximately 3" in diameter at its widest point. GenMAV is a bank-to-turn vehicle controlled by a pair of elevons that make up 50% of the chord on the horizontal stabilizer. Its body and wings are comprised of carbon fiber with enough layers to ensure adequate rigidity. For this investigation, the GenMAV is modeled with conventional ailerons, elevator, and rudder, a different control configuration from the actual hardware design. GenMAV was developed as a reference vehicle for research conducted within and outside of AFRL.[17] The generic design is based on several iterations of MAVs previously studied in AFRL and provides a convenient baseline from which various MAV technologies can be explored.[18]

Control system modeling of the flight vehicle was accomplished in the Matlab Simulink$^{TM}$environment. The 6DOF simulation environment was constructed using a direct implementation of the quaternion dynamics model documented by Phillips.[19,20] To provide aerodynamic disturbances, the continuous Dryden turbulence model within the Aerospace Blockset was used, with the wind speed parameter set to approximately 10 percent of the MAV ground speed. Characterization of the GenMAV vehicle, in order to provide an aerodynamic truth model, was accomplished with the Athena Vortex Lattice (AVL) code. AVL was developed by Harold Youngren of MIT, and subsequently by Mark Drela (also of MIT) to provide aerodynamic and flight-dynamic analysis of rigid aircraft with arbitrary configurations.[21] The program applies thin airfoil theory to predict the inviscid aerodynamic forces and moments acting on the lifting surface of an air vehicle. Thin airfoil theory approximates the airfoil as a combination of uniform flow and a vortex sheet placed along the camber line. This leads to the aerodynamic force and moment being primarily a function of angle of attack and camber line geometry. Based on the assumptions behind thin airfoil theory, AVL is best suited for applications involving thin lifting surfaces, i.e., maximum thickness of 12% chord or less, at small angles of attack and sideslip. In AVL, the lifting surfaces of an aircraft are modeled as single-layer vortex sheets discretized into horseshoe vortex filaments. Flow is assumed to be quasi-steady and within the limit pertaining to small reduced frequency. This

translates into the following limits for each of the dimensionless flow rate parameters:

$$-0.10 < \frac{pb}{2V} < 0.10$$
$$-0.03 < \frac{qc}{2V} < 0.03$$
$$-0.25 < \frac{rb}{2V} < 0.25.$$

Given that thin airfoil theory deals with 2-D potential flow, drag due to viscous effects is not calculated in AVL, and the lift coefficient is a linear function of angle of attack. Overall drag is represented as a combination of lift-induced drag plus an approximation for parasitic effects. In addition to static coefficients, AVL provides damping coefficients, including the coupled terms between roll and yaw, and control surface derivatives. The full complement of aerodynamic coefficients was used for this work.

For demonstration of the benefits of torque feedback, the attitude control was implemented using three independent PD controllers; body rate and attitude error were assumed to be optically observable. Pitch angle was used directly to control altitude error. The outer altitude control loop was in the form of PID control, allowing the integral term to account for gravity bias. The attitude loops were tuned to respond as critically damped second order systems with nominally a 5 Hz natural frequency. Attitude control output was in the form of a torque command for each body axis; i.e.,

$$\begin{aligned} Commanded\,Torque &= J\ddot{\theta} \\ &= -J\omega_n^2(\theta_m - \theta_{com}) - J2\zeta\omega_n\dot{\theta}_m \\ &= -K_p(\theta_m - \theta_{com}) - K_d\dot{\theta}_m, \end{aligned} \tag{1}$$

where $K_p$ and $K_d$ are the proportional and derivative control gains, $\theta$ is an angular degree of freedom with an associated inertia $J$. The desired damping ratio and natural frequency are represented by $\zeta$ and $\omega_n$, respectively.

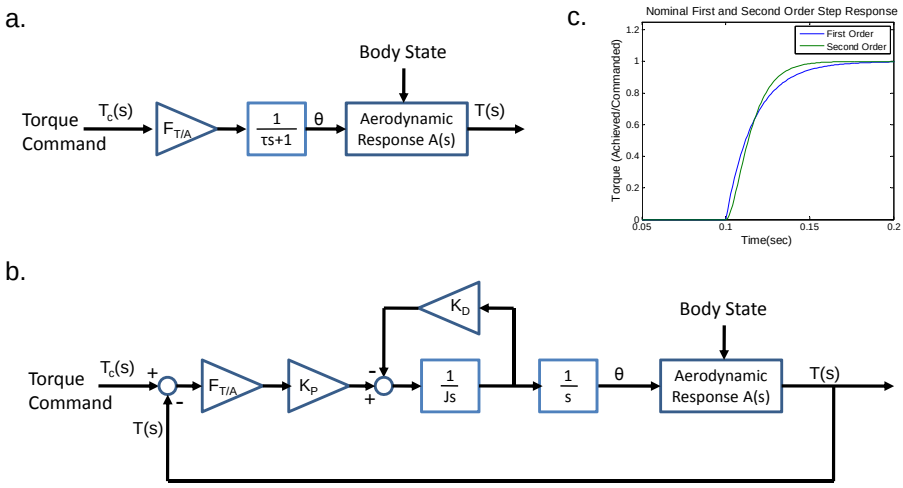


**Figure 3. Actuator response models used for load feedback 6DOF demonstrations: a) first order response model, b) second order torque error regulator. The nominal response time constants for both models were defined to be 17 ms as shown in c). In a) and b), $\theta$ represents the achieved control surface deflection and $F_{T/A}$ represents a nominal scale factor to convert torque to control surface deflection angle.**

A nominal first order control surface actuator response model was used for baseline comparison. Alternatively, closed-loop actuators, which used measured body torque error to drive the ailerons, elevator, and rudder, were modeled as second order damped torque motors with angular limits at +/- 30 degrees. The natural frequency of the second order actuator control loop was nominally 20 Hz, having a 17 ms time constant for 63% response. The first order actuator was also defined with a 17 ms time constant for consistency. Both actuator response models used a common scale factor, $F_{T/A}$, derived around straight and level flight conditions to convert torque to angle, Figure 3. Under nominal conditions, to the degree that the second and first order responses were similar, the airframe response would be expected to be similar. Under conditions of degraded control realization and non-zero latency, significant differences

would be expected due to the inability of the controller without torque feedback actuation to reflexively respond to errors and disturbances.

To demonstrate the potential benefit from augmenting the attitude controller with wing load feedback, a formulation was derived to use the assumed low-latency measurement of body torque to compensate for the destabilizing influence of high latency in the optical feedback pathway. To derive the control expression used, both inertia and feedback latency are assumed to be known to some approximation. The control gains associated with measured angle, $\theta_m$, angular rate, $\dot{\theta}_m$, and torque, $T_m$, are required:

$$Commanded\,Torque = -\bar{K}_p(\theta_m - \theta_{com}) - \bar{K}_d\dot{\theta}_m, -\bar{K}_t T_m.$$

These new gains are found in terms of the gains in (1), the latency, $\Delta t_{opt}$, and the inertia, $J$, using simple Taylor series approximations:

$$\dot{\theta}_{est} = \dot{\theta}_m + \frac{T_m}{J}\Delta t_{opt} \tag{2}$$

$$\begin{aligned}\theta_{est} &= \theta_m + (\dot{\theta}_m + \frac{T_m}{J}\Delta t_{opt})\Delta t_{opt} + \frac{T_m}{2J}\Delta t_{opt}^2 \\ &= \theta_m + \dot{\theta}_m\Delta t_{opt} + \frac{3T_m}{2J}\Delta t_{opt}^2.\end{aligned} \tag{3}$$

Substituting the estimates represented by (2) and (3) for the measured quantities in (1), then collecting terms, provides the following expressions for the new gains:

$$\bar{K}_p = K_p \tag{4}$$

$$\bar{K}_d = (K_p\Delta t_{opt} + K_d) \tag{5}$$

$$\bar{K}_t = \left(K_p\frac{3\Delta t_{opt}^2}{2J} + K_d\frac{\Delta t_{opt}}{J}\right). \tag{6}$$

Efforts to develop an optimal attitude control law using body force states to minimize a cost function, as in LQR, were not complete at the time of this publication.

## III. Results

Two test cases were devised to demonstrate the benefit of load sensing on dynamic performance. Both test cases included the turbulence model previously described and an initial one meter step command in altitude. The first test case demonstrated performance with and without degraded control response. To model the degraded control response, the angular response of all control surfaces was cut in half, thereby modeling a 50% degradation in control surface effectiveness. Linear forces through the center of gravity were not degraded.

Figures 4a and 4b show the roll and yaw attitude in the presence of turbulence and a one meter altitude step command with no torque feedback. The two time histories represent cases with and without control system degradation. Figures 4c and 4d show the same two cases with torque feedback to control actuator position. The cases with torque feedback to the actuator show roughly an order of magnitude better disturbance rejection. Both with and without torque feedback, an increase in attitude response is seen as a result of the control surface degradation. Figure 5 demonstrates the increased response of the rudder and aileron in the presence of control degradation without torque feedback, a) and b), and with torque feedback, c) and d). The control surface positions are similar in character with increased amplitude for the torque feedback control. As demonstrated by Figure 4, the closed-loop actuator more effectively dealt with the deviations from the commanded body torques.

The second test case involves introduction of latency into the state feedback that drives the attitude control law. In animal systems, in particular those that do not have highly dedicated rate sensing physiology, optical flow provides a primary means for sensing angular motion. In insects, the neuronal processing of vision motion may introduce 30 ms or more latency into the feedback process, depending on species and ambient light level. This delay would be expected to have a detrimental impact on the attitude control system. The strain mechanosensors typically have a much more direct pathway to the muscles that they stimulate. Campaniform sensilla, the load sensors on insects, can induce a response in the muscles in an order of magnitude less time than that achieved by the vision system. The haltere to motor neuron pathway in dipertan insects is a well characterized example of this type of quick reflexive response. For this test case, a latency of 3 ms on the torque feedback and 10 ms on the optical feedback was sufficient to demonstrate the benefit of closed-loop torque regulation.

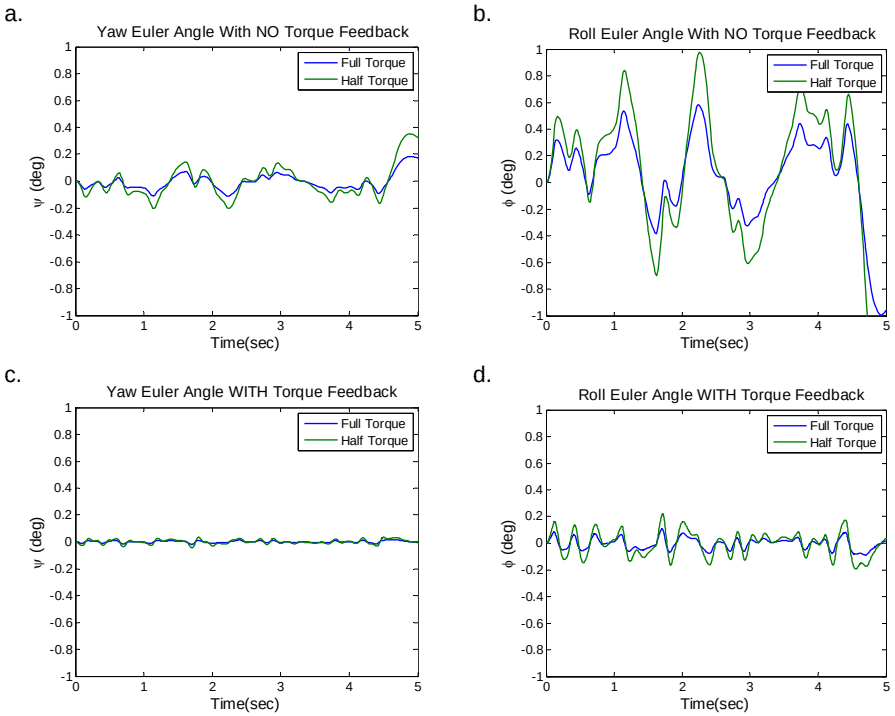


**Figure 4. Euler angle response of GenMAV without and with torque feedback to actuators for the case of 50% degradation in control capability. a) Yaw Euler angle with open-loop rudder control. b) Roll Euler angle with open-loop aileron control. c) Yaw Euler angle with torque feedback to rudder control. d) Roll Euler angle with torque feedback to aileron control.**

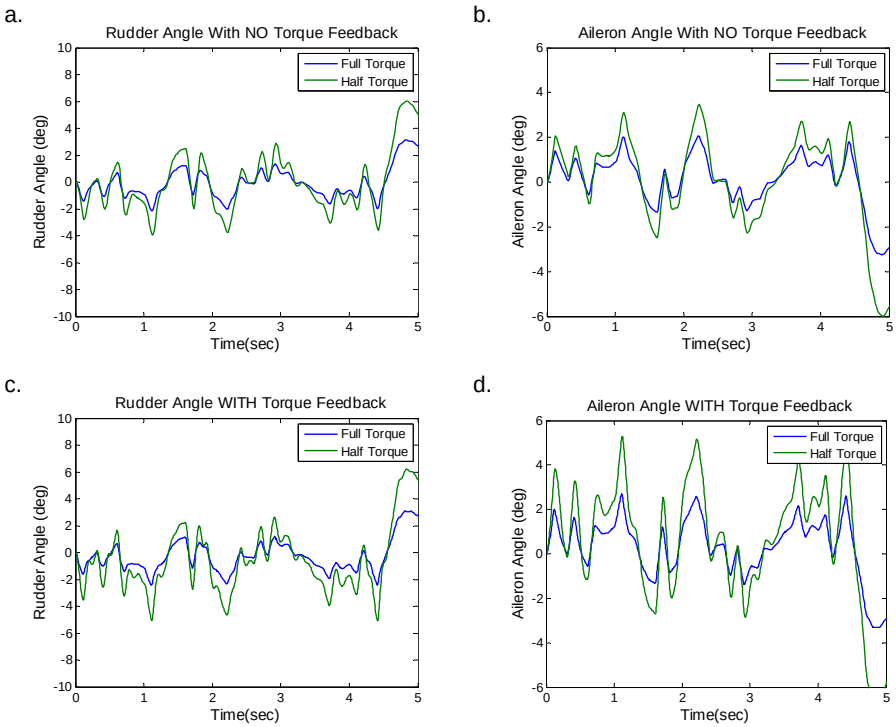


**Figure 5. Rudder and aileron control surface response for the case of 50% degradation in control capability (Figure 3). a) Open-loop rudder response and b) open-loop aileron response. c) and d) show response of the rudder and aileron with closed-loop actuator control.**

Figures 6a and 6b demonstrate that, without torque feedback, a highly oscillatory yaw and roll attitude response results in the presence of 10 ms of latency. This response is stimulated by turbulent disturbances. Note that the bandwidths of the attitude loops were tuned for the ideal zero latency case. In contrast, Figures 6c and 6d show the same comparison with the torque feedback to the actuators. Figure 7 shows the corresponding control surface angles for the two cases from Figures 6c and 6d. The two curves in this figure depict a very similar response. The fact that actuator response does not change significantly in the presence of the optical feedback latency indicates that the torque feedback loop is primarily responsible for mitigating the effect of the turbulence induced torque disturbances. The improved disturbance rejection delays the onset of system oscillation as latency increases.

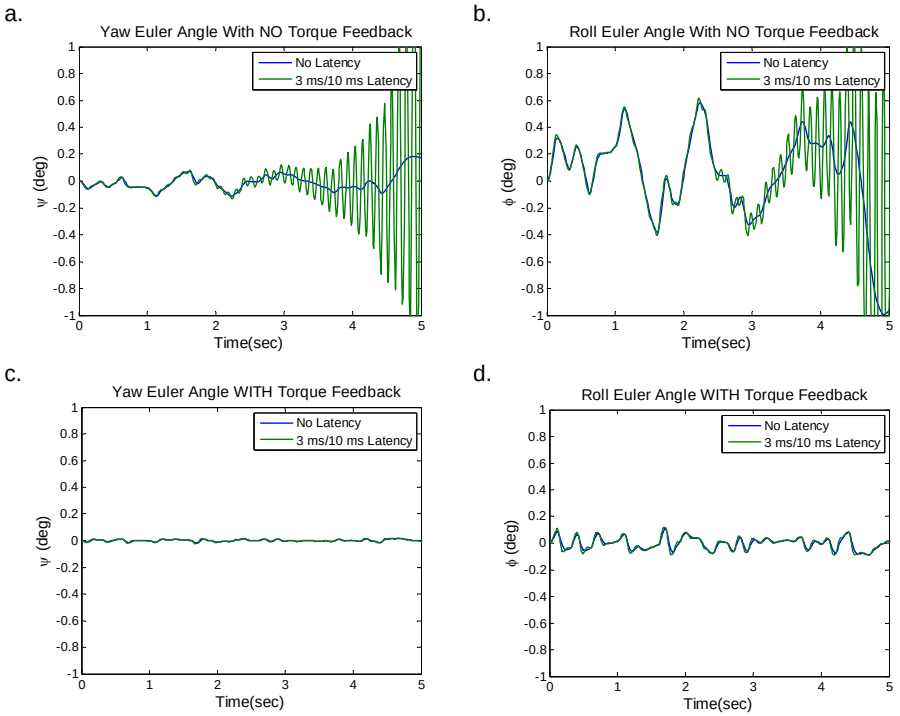


**Figure 6. Euler angle response of GenMAV without and with torque feedback to the actuators for the case of 3 ms torque feedback latency and 10 ms attitude state feedback latency. a) Yaw Euler angle with open-loop rudder control. b) Roll Euler angle with open-loop aileron control. c) Yaw Euler angle with torque feedback to rudder control. d) Roll Euler angle with torque feedback to aileron control.**

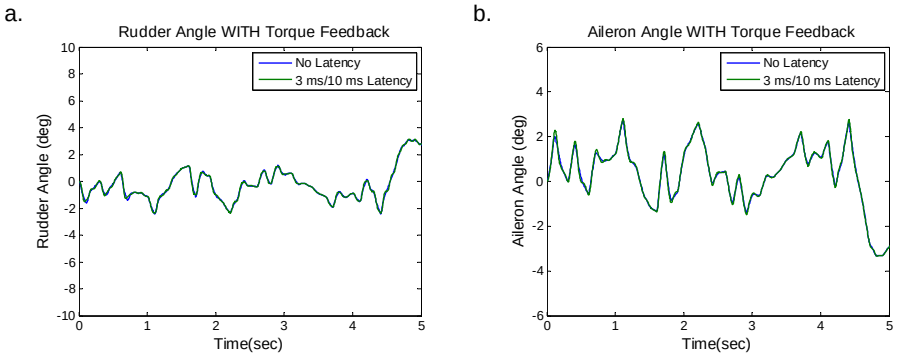


**Figure 7. Rudder and aileron control surface response for the case of 3 ms torque feedback latency and 10 ms attitude state feedback latency (Figures 6c and 6d). a) Open-loop control and b) torque regulated control.**

As latency increases further, even with torque feedback to the actuator, the system begins to destabilize as shown in Figure 8a. In this example, 30 ms of latency was simulated. Figure 8b shows the response with the PD attitude controller augmented with torque to compensate for the latency (PDT control), reference equations (4)-(6). In this case, the system responds with some pitch oscillation in response to the one meter step in altitude, but quickly stabilizes,

closely matching the zero latency baseline case. Note that the motion that dominates in all cases described is pitch motion. There is no mechanism in the defined control scheme to respond to measured z-force error except through pitch control. The resulting motion to affect a decrease in altitude error is much larger than the residual motion in yaw and roll. In a flapping wing design, where z-force could be controlled independently, this coupling of degrees of freedom would not necessarily be required.

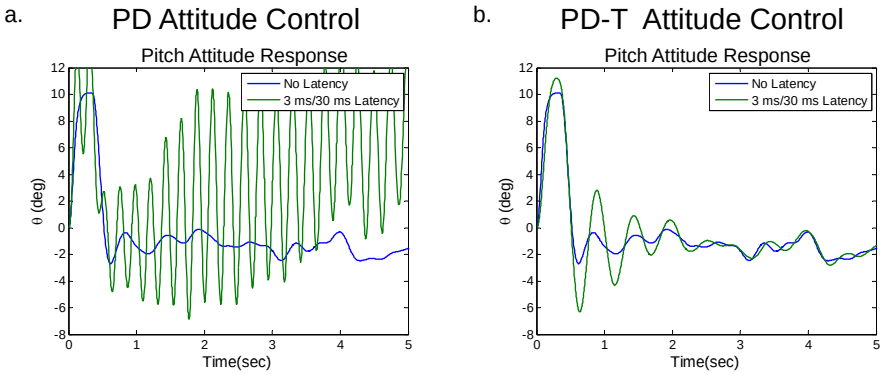


**Figure 8. Pitch response for the case of 30 ms optical latency and closed-loop actuator control. Figure a) shows the highly oscillatory nature of the response without latency compensation. Figure b) shows the improved response with torque augmented attitude control to compensate for the latency.**

## IV. Discussion

The results in this paper demonstrate the ability of wing load sensors to improve attitude control robustness and disturbance rejection in the presence of significant uncertainty in plant characteristics. By directly measuring the torque around a given axis, the error with respect to the torque commanded by the attitude control law can be reduced without dependence on known aerodynamic characteristics of the airframe. Through the same mechanism, torque disturbances on the airframe can be dealt with through high speed reflexive control, leaving the outer attitude control loop to deal with lower frequency optical tracking. This wing load feedback mechanism may explain the robustness of insect flight, where significant damage to wings is tolerated and high variations in control performance occur due to such factors as temperature, age, individual variation, and metabolic state.

The results shown in this paper rely on many assumptions with respect to sensor implementation. Actual implementation of strain sensors may be a significant hurdle to realization of the results shown. Nature has evolved systems that rely on large numbers of simple sensors spread throughout the body structure to sense and respond to interaction with the environment. While individual sensors may be very poor detectors of magnitude, in concert, a number of simple sensors spread throughout a structure might have a very large effective dynamic range. The human engineering approach is to build more elaborate sensors that individually achieve the required dynamic range. Inherent in these approaches is a trade-off between integration complexity and robustness to damage. If one of the many simple sensors associated with the insect wing is not functional, a small price is paid in terms of overall dynamic range, but the system still functions. If the single, more elaborate sensor on the man-made system is damaged, the result might be catastrophic. Significant engineering development in materials and manufacturing technology would be required to duplicate the design paradigm that is prevalent in natural systems. However, similar performance characteristics might be achievable by mimicking a low-latency, load-based control mechanism without duplicating the sophistication in materials and manufacturing seen in nature.

To achieve the results shown, either strain sensors would have to be placed near the body on the aero surfaces, or the angular acceleration of the body would need to be measured directly. With knowledge of the body inertia characteristics, the net torques on the body could be deduced from the angular accelerations. The feedback to the modeled closed-loop actuator is an assumed estimate of the net torque on the body. The calculations and calibrations required to realize actual quantitative estimates of torque around the center of gravity could become very elaborate. Clearly, nature is not explicitly relying on quantitative estimates of torque around the center of gravity. Natural designs take maximum advantage of symmetry and the differential effect of control force application across the plane of symmetry. In fact, strain sensors on the left half of the body may influence left wing control, while sensors on the right half influence right wing control, without a significant contralateral influence, as in the halteres of flies. The

net effect of the forces would still result in a stabilizing influence. The primary requirement is a signal, related to the net torque on the body, that can be driven to zero or to a correctly biased state, thereby driving the torque error to zero. This should be achievable with symmetric placement of strain sensors on the right and left aero surfaces. Compensation for residual biases can be realized through appropriate application of controller integral terms and the aerodynamic stability inherent in the basic design.

The fundamental idea of using feedback to eliminate uncertainty in the output of an actuator is not new. For example, hydraulic torque motors are sometimes implemented with a pressure loop around the valve to reduce the impact of hydraulic resonance. The same technique is more generally used to eliminate nonlinearities in open-loop actuator response. Treating the entire airframe as a torque motor with the error driving the control surface state is a deviation from conventional attitude control techniques. The requirement for a fail-safe feature, in case of feedback interruption, must be taken into consideration; lacking a feedback signal, the control surfaces will be driven to the limits in an attempt to reduce the error.

The techniques described in this paper might allow for MAV designs that come closer to the performance and robustness of natural systems. An additional objective of this research is decreased cost and complexity of MAV designs. Obtaining this goal is dependent upon replacement of more costly or complex rate sensors. This described control technique relies on the ability to implement the strain or load sensing transducers and the ability to obtain the requisite outer loop rate and tracking estimates from multi-use optical sensors. This objective configuration mimics many insect sensor architectures. Nature is clearly able to achieve remarkable agility, behavioral complexity, and robustness in extremely small packages through mechanisms that scientists and engineers are only beginning to understand. The human tendency to attribute undue complexity to systems that we do not understand should be considered. A concept as simple as reflexive response to wing load sensing could potentially explain much about the robustness and performance capability seen in natural flying systems.

## Acknowledgments

The Air Force Office of Scientific Research (AFOSR) has been a long standing proponent of research into the physiological and behavioral mechanisms of natural systems. In particular, Dr. Willard Larkin has facilitated this work through his financial support and keen insight into productive areas of research. The Munitions Directorate, AFRL/RW, has also had the foresight to allow foundational research into biomimetic technologies, resulting in a unique group of engineers, physicists, and biologists performing ground breaking investigations in the areas of agile autonomous systems and alternative navigation. The authors would also like to acknowledge Mr. David New for his help in graphical visualization of simulation results.

## References

[1]Collett, T. S., "Insect Navigation: Visual Panoramas and the Sky Compass," *Current Biology*, Vol. 18, No. 22, 2008, pp. R1058–R1061.

[2]Collett, M., Collett, T. S., and Srinivasan, M. V., "Insect Navigation: Measuring Travel Distance across Ground and through Air," *Current Biology*, Vol. 16, No. 20, 2006, pp. R887–R890.

[3]Floreano, D., Zufferey, J., Srinivasan, M., and Ellington, C., "Flying Insects and Robots," *Flying Insects and Robots*, Springer-Verlag, 2009, ISBN 978-3-540-89392-9.

[4]Humbert, J. S. and M., H. A., "Bioinspired visuomotor convergence," *IEEE Transactions on Robotics*, Vol. 26, 2010, pp. 1552–3098.

[5]Taylor, G. K. and Krapp, H. G., "Sensory Systems and Flight Stability: What do Insects Measure and Why?" *Advances in Insect Physiology*, Vol. 34, Elsevier Ltd., 2007, pp. 231–316.

[6]Rutkowski, A. J., *Wind-borne Odor Tracking in Three Dimensions: A Biologically-inspired Sensor Fusion Approach*, VDM Verlag, 2008.

[7]Barth, F. G. and Humphrey, Joseph A.C.and Secomb, T. W., editors, *Sensors and Sensing in Biology and Engineering*, Springer, 2003.

[8]Pringle, J. W. S., "The gyroscopic mechanism of the halteres of Diptera," *Philos Trans R Soc Lond [Biol]*, Vol. 233, 1948, pp. 347–384.

[9]Thompson, R. A., Wehling, M. F., Evers, J. H., and Dixon, W. E., "Body rate decoupling using haltere mid-stroke measurements for inertial flight stabilization in Diptera," *J Comp Physiol A*, Vol. 195, 2009, pp. 99–112.

[10]Thompson, R. A., Rummelt, N., and Dixon, W. E., "Angular Rate Encoding in Haltere Feedback for Flight Stabilization of Dipteran Insects," *AIAA Guidance, Navigation, & Control Conference, Chicago, IL*, 2009.

[11]Krapp, H. G., "Sensorimotor transformation: from visual responses to motor commands," *Curr Biol*, Vol. 20, 2010, pp. R236–R239.

[12]Dickinson, M. H., "Comparison of Encoding Properties of Campaniform Sensilla on the Fly Wing," *J. Exp. Biol.*, Vol. 151, 1990, pp. 245–261.

[13]Zill, S. N. and Moran, D. T., "The Exoskeleton and Insect Proprioception. I. Responses of Tibial Campaniform Sensilla to External and Muscle Generated Forces in the American Cockroach, Periplaneta Americana," *J. Exp. Biol.*, Vol. 91, 1981, pp. 1–24.

[14]Dickinson, M. H., Hannaford, S., and Palka, J., "The Evolution of Insect Wings and Their Sensory Apparatus," *Brain Behav Evol*, Vol. 50, 1997, pp. 13–24.

[15]Elson, R. C., "Interneuronal processing of inputs from the campaniform sensilla of the locust hindwing," *J. Comp Phys. A*, Vol. 161, 1987, pp. 761–776.

[16]Dickinson, M. H., "The Initiation and Control of Rapid Flight Maneuvers in Fruit Flies," *Integr. Comp. Biol.*, Vol. 45, 2005, pp. 274–281.

[17]Stewart, K., Wagener, J., Abate, G., and Salichon, M., "Design of the Air Force Research Laboratory Micro Aerial Vehicle Research Configuration," *AIAA 45th Aerospace Sciences and Meeting Exhibit*, 2007.

[18]Stewart, K., Blackburn, K., Wagener, J., Czabaranek, J., , and Abate, G., "Development and Initial Flight Tests of a Single-Jointed Articulated-Wing Micro Air Vehicle," *AIAA Atmospheric Flight Mechanics Conference*, 2008.

[19]Phillips, W. F., Hailey, C. E., and Gebert, G. A., "A Review of Attitude Representations Used for Aircraft Kinematics," *Journal of Aircraft*, Vol. 38, No. 4, 2001, pp. 718–737.

[20]Phillips, W. F., *Mechanics of Flight, 2nd Edition*, Wiley, Hoboken, NJ,, 2010.

[21]Drela, M. and Youngren, H., "Athena Vortex Lattice (AVL) Software Package, Ver 3.27," http://web.mit.edu/drela/Public/web/avl/.

# Cooperative Defense within a Single-Pursuer, Two-Evader Pursuit Evasion Differential Game

Zachariah E. Fuchs*
Department of Electrical and Computer Engineering
University of Florida

Pramod P. Khargonekar**
Department of Electrical and Computer Engineering
University of Florida

Johnny Evers
AFRL/RWAV, Eglin AFB,
Florida 32542-6810, USA

***Abstract*— This paper is motivated by a desire to develop analytical formulations for cooperative defensive strategies against predator(s). We formulate a single-pursuer, two-evader differential game with a novel cost functional. Each of the three agents are modeled as massless particles that move with constant velocity. The pursuer attempts to capture either of the evaders while minimizing its cost. Simultaneously, the evaders strive to maximize the pursuer's cost. The proposed cost functional represents the increased cost to the pursuer when presented with multiple, potentially dangerous targets. It captures the effect of cooperation between the evaders. In order to solve the game, we develop the optimality conditions for the equilibrium strategies. We then integrate the resulting system of ordinary differential equations backwards in time from the terminal conditions to generate the optimal trajectories of the three agent system. The resulting trajectories display cooperative behaviors between the two evaders, which are qualitatively similar to behaviors found in predator-prey interactions in nature. Brief description of singular surfaces is also included.**

## I. Introduction

The use of unmanned mobile systems is rapidly increasing due to a variety of reasons including their relative low cost and their ability to operate in hazardous environments with minimal risk to human life. Multiple cheap unmanned systems, or agents, can be deployed simultaneously to accomplish a task or mission. A very important application of unmanned systems is in the modern battlefield to perform tasks ranging from surveillance to direct engagement. In these scenarios, the group of agents are often in direct competition with an opposing force. It is therefore important to find algorithms or strategies that can systematically maximize the value offered by such groups of agents.

A natural setting for studying such issues is game theory. In this paper, we introduce a single-pursuer, two-evader game with a novel integral cost functional. This cost functional is intended to represent the risk of damage or injury to the pursuer or the additional energy or computational expense needed to monitor multiple evaders. During the game, the pursuer strives to minimize this cost while attempting to capture one of the evaders. Simultaneously, the evaders attempt to maximize the pursuer's cost in the hopes of making pursuit unattractive from certain initial conditions, thereby protecting themselves and their fellow evader. The proposed cost functional is a combination of a constant time penalty and evader generated cost. The evader generated cost component is based on the relative configuration of the three agents and possesses particular characteristics that encourage the evaders to attempt flanking maneuvers to surround the pursuer. As a direct result of the evader generated cost component, the optimal evader strategies exhibit cooperative defensive behaviors. It should be noted that cooperation is not directly imposed as a requirement of the solution. Instead, cooperation emerges as the optimal strategy.

The cooperative behaviors exhibited in the solution to this game are qualitatively similar to numerous examples of prey strategies used in response to attacking predators. Some examples include red-wing black bird nest defense [1], meerkat predator mobbing [2], and predator identification in guppy schools [3]. Such animal behaviors have been studied extensively within the biological community, and theories that explain their evolutionary stability and advantages have been proposed [4]. Often, these theories utilize principles from game theory. In particular the concept of repeated games is commonly deployed for this purpose [5], [6]. In these approaches, the potential behaviors are represented as strategies with assigned utilities that are inferred from empirical data or based on the genetic similarity between individuals. The different strategies are then shown to increase the survivability or fitness of the genes that describe these behaviors over time or multiple generations. Although these approaches explain how cooperation is optimal in the evolutionary sense, they do not directly address how cooperation is beneficial at the day-to-day, system level. One goal of this paper is to show how cooperation can arise as the optimal strategy given particular system dynamics and cost functional.

Although biologically inspired, our main motivation for the the scenario presented in this paper and the resulting cooperative defensive behaviors comes from the idea of cooperative defense of high value assets. Just as in nature, there are rarely any defenseless targets, and attacking forces usually elect not to attack a target if the potential for injury or high cost outweighs the benefit of the attack mission. Thus, by cooperating to combine their defensive resources, a group of evaders can make engagement more costly to the attacker than if they acted independently. This increased cost may then surpass a tolerance level for the potential attacker and prevent an attack before it ever occurs. For example,

*This material is based upon work supported under a National Science Foundation Graduate Research Fellowship to Zachariah Fuchs.

**Pramod P. Khargonekar was supported by the Eckis Professor endowment at the University of Florida.

through cooperation a group of unmanned drones could be used to protect vulnerable high-value targets, such as slow moving cargo planes, supply ships, or a very important person. If the high value target was attacked, the drones could then engage in a cooperative defensive maneuver. This cooperative defensive maneuver could be sufficient to protect the intended asset.

Formally introduced by Isaacs [7], pursuit-evasion games and their variants have been used to solve a wide range of problems. Recently, the authors in [8] use the same analysis techniques of this paper to examine a continuous time, visibility based, single-pursuer, single-evader game in an environment containing polygonal obstacles. There have been several papers that focused on combat with realistic dynamics [9], [10]. Pursuit-evasion games have also been used to generate defensive strategies of a single evader. In [11], the authors determine the optimal strategies for electronic counter measure use when initial conditions are known. Because of the ability to optimize multiple and sometimes conflicting value functions, game theory lends itself to the analysis of cooperative systems. In [12], the authors modify Isaacs' standard single-pursuer homicidal chauffeur game by allowing multiple pursuers and propose a daisy-chain formation that enables capture for a wider range of parameters. A multi-evader pursuit evasion game was posed in [13], but the cost functional was based solely on elapsed time. Because there was no direct cost generated by the evaders, the resulting evader behaviors exhibit a scattered, fleeing pattern instead of a cohesive, cooperative defensive strategy as seen in our formulation. The situation in which the evader can potentially capture or harm the pursuer is also presented in [14] and [15].

In Section II, we describe the system under consideration. We also develop an alternative coordinate system, which will simplify later analysis. A novel evader generated cost function is then developed that captures the synergy between the two evaders and serves as the primary motivation for cooperation. Using the developed instantaneous cost, we then describe the pursuit evasion game under analysis. In Section III, we develop the optimality conditions and perform the necessary integration to generate the optimal agent trajectories. Finally, in Section IV we summarize our findings and describe future research directions.

## II. SYSTEM AND GAME FORMULATION

In this section, we will describe the three agent system under analysis and define the kinematic equations that control their motion. We will also introduce a relative coordinate system and corresponding kinematic equations, which will prove to be more compact and intuitive for our analysis. After the system kinematics are defined, we develop an integral cost function which is based on the relative configuration of the three agents. In the third section, we lay out the motivations for a two-team differential game using the defined system kinematics and pursuer cost function.

### A. Kinematics of Agents

Consider a dynamic system with three agents: two evaders and a pursuer. For brevity, we will often refer to the two evaders as $E_1$ and $E_2$ and the pursuer as P. The three agents are modeled as massless particles moving with simple motion about an obstacle-free, infinite plane. Within this paper, two different but equivalent coordinate systems are used. The first coordinate system is referred to as the *global* coordinate system and will be used to plot agent trajectories and other visualizations. In this coordinate system, the position of each agent is defined by its own pair of standard Cartesian coordinates $(x,y)$. The velocities of $E_i$ $i=(1,2)$ and P are defined as $(v_i,\hat{\theta}_i)$ and $(v_p,\hat{\psi})$ respectively. Here $v_i$ and $v_p$ represent the magnitude of velocities and $\hat{\theta}_i$ and $\hat{\psi}$ represent the heading. The heading angles are measured counter-clockwise from the positive x-direction. The heading angle is the control variable for each agent, and we assume $v_i$ and $v_p$ are constant. The state of system is completely defined by the 6-tuple, $\mathbf{x}_G=(x_1,y_1,x_2,y_2,x_p,y_p)$. The global coordinate system is depicted graphically in Fig. 1a. The global kinematic equations of the system are thus

$$\begin{aligned} \dot{x}_p &= v_p\cos\hat{\psi} & \dot{y}_p &= v_p\sin\hat{\psi} \\ \dot{x}_1 &= v_1\cos\hat{\theta}_1 & \dot{y}_1 &= v_1\sin\hat{\theta}_1 \\ \dot{x}_2 &= v_2\cos\hat{\theta}_2 & \dot{y}_2 &= v_2\sin\hat{\theta}_2 \end{aligned} \tag{1}$$

We will now introduce a second coordinate system, which will represent the locations of each of the evaders relative to the position of the pursuer. This representation will allow us to reduce the number of dimensions in later analysis and will be referred to as the *relative* coordinate system. In this coordinate system, the state of the system is represented by the following 6-tuple, $\mathbf{x}_R=(d_1,d_2,\alpha,\beta,x,y)$. The first two coordinates, $d_1$ and $d_2$, represent the distance between $E_1$ and P and the distance between $E_2$ and P respectively. The angle $\alpha$ is measured counter-clockwise from $\overrightarrow{PE_1}$ to $\overrightarrow{PE_2}$. The angle $\beta$ represents the global rotation of the three agent system and is measured counter-clockwise from the positive x-direction to $\overrightarrow{PE_1}$. The x and y coordinates represent global position of the pursuer. The six coordinates can be separated into two groups. The first group, $(d_1,d_2,\alpha)$, contains all necessary information to describe the relative configuration of the three agents. The second group, $(\beta,x,y)$, contains the global rotational and translation information. In the relative coordinate system, the evader heading angle, $\theta_i$, is measured counter-clockwise from $\overrightarrow{PE_i}$ in order to simplify the kinematic equations. Similarly, the pursuer heading angle, $\psi$, is measured counter-clockwise from $\overrightarrow{PE_1}$. The relative coordinate system is graphically depicted in Fig. 1b.

The global and relative representations are related through the following equations.

$$x_p = x \qquad y_p = y \tag{2}$$

$$x_1 = d_1\cos(\beta)+x \qquad y_1 = d_1\sin(\beta)+y \tag{3}$$

$$x_2 = d_2\cos(\beta+\alpha)+x \qquad y_2 = d_2\sin(\beta+\alpha)+y \tag{4}$$

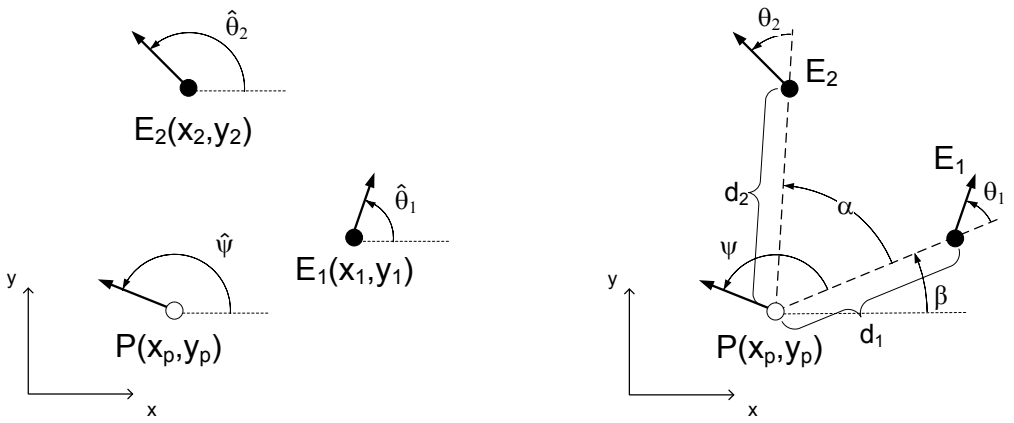


(a) Global Coordinates (b) Relative Coordinates

Fig. 1. Coordinate Systems

The control variables are related as follows.

$$\hat{\theta}_1 = \theta_1 + \beta \quad \hat{\theta}_2 = \theta_2 + \beta + \alpha \quad \hat{\psi} = \psi + \beta \tag{5}$$

Using the variables in the reduced model with the dynamics in (2), the reduced space kinematic equations are shown below.

$$\dot{d_1} = v_1 \cos\theta_1 - v_p \cos\psi \tag{6}$$

$$\dot{d_2} = v_2 \cos\theta_2 - v_p \cos(\psi - \alpha) \tag{7}$$

$$\dot{\alpha} = \tfrac{v_2}{d_2} \sin\theta_2 - \tfrac{v_1}{d_1} \sin\theta_1 + v_p \left( \tfrac{1}{d_1} \sin\psi - \tfrac{1}{d_2} \sin(\psi - \alpha) \right) \tag{8}$$

$$\dot{\beta} = \tfrac{1}{d_1} (\sin\theta_1 - v_p \sin\psi) \tag{9}$$

$$\dot{x} = v_p \cos(\psi + \beta) \tag{10}$$

$$\dot{y} = v_p \sin(\psi + \beta) \tag{11}$$

We further condition these equations with the following two restrictions.

$$d_1 \geq d_c \quad \text{and} \quad d_2 \geq d_c \tag{12}$$

$$v_1 < v_p \quad \text{and} \quad v_2 < v_p \tag{13}$$

The first restriction, (12), requires that both distances are greater than or equal to the capture distance, $d_c$. The second restriction, (13), requires that the pursuer is faster than both of the evaders, which ensures that the pursuer is capable of capturing an evader in finite time.

### *B. Instantaneous Cost Function*

In this section, we develop an instantaneous cost function dependent on the relative positions of the two evaders and pursuer. The developed cost function captures the synergy between the evaders and serves as the primary incentive for cooperation within the evading team. With respect to our biological inspiration, this cost could model the risk of injury to a predator caused by the prey. In terms of a man-made example, the evader-generated cost could represent the risk of damage to an attacking aircraft from the targets' defensive capabilities.

Each evader generates an individual cost, which is a function of distance between the evader and pursuer. In this paper, exponential cost functions are used for $E_1$ and $E_2$:

$$C_1(d_1) = k_1 e^{k_2(d_c - d_1)} \ , \ C_2(d_2) = k_1 e^{k_2(d_c - d_2)} \tag{14}$$

where the constant $k_1$ defines the maximum value of the cost and $k_2$ controls how quickly the cost decays as a function of distance. These functions were chosen because of their simplicity, but more complex functions could be used to model particular predator-prey or attacker-target interactions.

We provide the pursuer the ability to counteract or reduce these individual costs. Returning to our aircraft attack example, the aircraft may be able to perform evasive maneuvers or deploy countermeasures if a threat is detected. The detection of the threat may be relatively straightforward if only a single target exists, but in the case of multiple targets, it may be necessary to allocate finite sensory or processing capabilities between multiple threats. The decreased vigilance of the targets at the individual level increases the overall risk of damage.

We model this effect by defining a direction of sensory focus, $\gamma$, for the pursuer. The direction of focus is independent of the motion of P and is measured counter-clockwise from $\overrightarrow{PE_1}$. By steering the direction of focus toward an evader, the pursuer reduces the cost generated by that evader. The resulting reduced costs are a product of the cost reduction function and the original evader cost:

$$C_{E_1}(\gamma, \mathbf{x}) = S(\gamma) C_1(d_1) \tag{15a}$$

$$C_{E_2}(\gamma, \mathbf{x}) = S(\gamma - \alpha) C_2(d_2) \tag{15b}$$

where $S(\cdot)$ represents the cost reduction as a function of the difference between the sensory focus angle and the angle towards the evader. In this paper we use the following definition for $S(\cdot)$.

$$S(\cdot) = \tfrac{1}{2} [1 - \cos(\cdot)] \tag{16}$$

The total evader-generated cost for the pursuer is the sum of the individual evader costs:

$$C_E(\gamma,\mathbf{x}) = C_{E_1}(\gamma,\mathbf{x}) + C_{E_2}(\gamma,\mathbf{x}) \tag{17}$$

The pursuer must then select $\gamma^*$ such that that the total cost is minimized at any moment in time. The minimizing $\gamma^*$ satisfies the following conditions

$$\cos\gamma^* = \tfrac{C_1+\cos(\alpha)C_2}{\rho} \quad \sin\gamma^* = \tfrac{\sin(\alpha)C_2}{\rho} \tag{18}$$

where

$$\rho = \sqrt{C_1^2 + 2C_1C_2\cos\alpha + C_2^2} \tag{19}$$

Substituting the optimal $\gamma$-strategy, (18)-(19), into (17) provides the minimum cost:

$$C_E(\gamma^*,\mathbf{x}) = \tfrac{1}{2}\Big[C_1 + C_2 - \sqrt{C_1^2 + 2C_1C_2\cos\alpha + C_2^2}\Big] \tag{20}$$

It should be noted that this function evaluates to zero when $\alpha = 0$. This situation allows the pursuer to monitor both evaders simultaneously. The evader cost function is maximized when $\alpha = \pi$, which represents the scenario in which the evaders have flanked the pursuer and it can only direct its beam of focus at the most costly pursuer.

Because $\gamma$ does not affect the system dynamics and the pursuer can instantaneously choose any value for $\gamma$, we will assume the pursuer always chooses $\gamma^*$. As a result, we will consider the instantaneous evader-generated cost as a function of state alone and no longer consider $\gamma$ in the development of the game. An additional constant cost term, $c_t$, is added to the evader-generated cost in order to represent a time or energy penalty for the pursuer. The total pursuer instantaneous cost is then

$$C_T(\mathbf{x}) = C_E(\mathbf{x}) + c_t \tag{21}$$

### C. Game Formulation

The instantaneous cost function (21) is integrated over time to calculate the total cost to the pursuer over a single play of the game. In this game, termination occurs when the pursuer captures one of the evaders, which happens when the state passes through the terminal surface:

$$\Gamma(\mathbf{x}) = (d_1 - d_c)(d_2 - d_c) = 0 \tag{22}$$

The cost to the pursuer for a game starting at initial time $t_0$ and reaching the terminal surface at time $t_f$ is then defined as:

$$J = \int_{t_0}^{t_f} C_E(\mathbf{x}) + c_t \;\; dt \tag{23}$$

We can now pose a differential game in which the goal of the two evaders is to maximize the integral cost to the pursuer, (23). By inspection, it can be seen that in general the evaders should strive to delay termination of the game in order to continue the integration of cost. Simultaneously, the the pursuer strives to minimize its cost my terminating the game as soon as possible while attempting to avoid potential flanking maneuvers of the evaders.

Although there are three agents in this system, the two evaders share a common goal, maximize the pursuer's cost. Therefore, the evaders can be thought of as a single player with two control variables. This perspective results in a two-player zero-sum game; one player is the pursuer, while the other player represents the evading team. We can then define a function $V(\mathbf{x})$, which represents the value of a game that starts at point $\mathbf{x}$ and in which both players implement their optimal strategies.

In this paper, we assume that all agents possess complete knowledge of all state variables. The pursuer does not possess knowledge of either evader's control while the evaders are ignorant of the pursuer's control as well.

## III. Solution to the Game

In this section we will develop the solution to the game. For this paper, we will examine the case where $v_1 = v_2 = 1$, $k_1 = k_2 = 1$, and $c_t > 0$. It is assumed that $t_0 = 0$. We will first calculate the optimality conditions that describe the optimal control strategies. Using the calculated optimality conditions, we numerically integrate backwards in time to generate the optimal trajectories. We will then discuss some of the interesting singular surfaces generated within the state-space and their effects on the optimal state trajectories. All of the following calculations are performed using the relative coordinate system.

### A. Optimality Conditions for the Game of Attack

In order to find the optimal control strategies and the resulting state trajectories, we begin by calculating the optimality conditions of differential games first described by Rufus Isaacs [7]. Using the defined kinematic equations, (7)-(11), and the cost functional (21), the Hamiltonian, H, is introduced as

$$\begin{aligned} H &= \lambda^T \mathbf{f}(\mathbf{x}, u_p, \mathbf{u_e}) + C_T \\ &= \lambda_1\dot{d_1} + \lambda_2\dot{d_2} + \lambda_\alpha\dot{\alpha} + \\ &\quad \lambda_\beta\dot{\beta} + \lambda_x\dot{x} + \lambda_y\dot{y} + C_T \end{aligned} \tag{24}$$

The vector $\lambda = \begin{pmatrix}\lambda_1 & \lambda_2 & \lambda_\alpha & \lambda_\beta & \lambda_x & \lambda_y\end{pmatrix}^T$ contains the adjoint variables conjugate to the kinematic equations. The adjoint equations are found by taking the partial derivative of the Hamiltonian with respect to their respective state component:

$$\dot{\lambda}_1 = -\tfrac{\partial H}{\partial d_1} = -\lambda_\alpha\tfrac{\partial\dot{\alpha}}{\partial d_1} - \tfrac{\partial C_T}{\partial d_1} \tag{25}$$

$$\dot{\lambda}_2 = -\tfrac{\partial H}{\partial d_2} = -\lambda_\alpha\tfrac{\partial\dot{\alpha}}{\partial d_2} - \lambda_\beta\tfrac{\partial\dot{\beta}}{\partial d_2} - \tfrac{\partial C_T}{\partial d_2} \tag{26}$$

$$\dot{\lambda}_\alpha = -\tfrac{\partial H}{\partial \alpha} = -\lambda_2\tfrac{\partial\dot{d_2}}{\partial\alpha} - \lambda_\alpha\tfrac{\partial\dot{\alpha}}{\partial\alpha} - \tfrac{\partial C_T}{\partial\alpha} \tag{27}$$

$$\dot{\lambda}_\beta = -\tfrac{\partial H}{\partial \alpha} = -\lambda_x\tfrac{\partial\dot{x}_p}{\partial\beta} - \lambda_y\tfrac{\partial\dot{y}_p}{\partial\beta} \tag{28}$$

$$\dot{\lambda}_x = -\tfrac{\partial H}{\partial x} = 0 \tag{29}$$

$$\dot{\lambda}_y = -\tfrac{\partial H}{\partial y} = 0 \tag{30}$$

The boundary conditions, $\Psi$, for the game are

$$\Psi = \begin{pmatrix} d_1(t_0) - d_{10} \\ d_2(t_0) - d_{20} \\ \alpha(t_0) - \alpha_0 \\ \beta(t_0) - \beta_0 \\ x(t_0) - x_0 \\ y(t_0) - y_0 \\ (d_1(t_f) - d_c)(d_2(t_f) - d_c) \end{pmatrix} = 0 \tag{31}$$

where $d_{10}$, $d_{20}$, $\alpha_0$, $\beta_0$, $x_0$, and $y_0$ are the initial values of their respective state components at the start of the game. In order to determine the boundary constraints on the adjoint variables, we use the boundary conditions, (31), to create a function of terminal conditions, $\Phi$:

$$\Phi = \nu^T \Psi \tag{32}$$

where $\nu = (\ \nu_1\ \ \nu_2\ \ \nu_3\ \ \nu_4\ \ \nu_5\ \ \nu_6\ \ \nu_7\ )^T$ contains the adjoint variables conjugate to the boundary constraints of the state. Taking the partial derivatives of (32) with respect to the state components provides the terminal conditions for the adjoint variables:

$$\lambda_1(t_f) = \tfrac{\partial \Phi}{\partial d_1(t_f)} = \nu_8(d_2 - d_c) \tag{33}$$

$$\lambda_2(t_f) = \tfrac{\partial \Phi}{\partial d_2(t_f)} = \nu_8(d_1 - d_c) \tag{34}$$

$$\lambda_\alpha(t_f) = \tfrac{\partial \Phi}{\partial \alpha(t_f)} = 0 \tag{35}$$

$$\lambda_\beta(t_f) = \tfrac{\partial \Phi}{\partial \beta(t_f)} = 0 \tag{36}$$

$$\lambda_x(t_f) = \tfrac{\partial \Phi}{\partial x(t_f)} = 0 \tag{37}$$

$$\lambda_y(t_f) = \tfrac{\partial \Phi}{\partial y(t_f)} = 0 \tag{38}$$

Using the adjoint derivatives, (28)-(30), and the terminal constraints, (36)-(38), it is found that

$$\lambda_\beta(t) = 0 \quad \lambda_x(t) = 0 \quad \lambda_y(t) = 0 \tag{39}$$

Substituting (39) into (24), results in a simplified Hamiltonian, which is dependent only on the components of the state that describe the relative configuration of the three agents:

$$H = \lambda_1 \dot{d}_1 + \lambda_2 \dot{d}_2 + \lambda_\alpha \dot{\alpha} + C_T \tag{40}$$

The next step in solving the game is to determine the optimal strategies for the three agents, which we will denote as $\theta_1^*$, $\theta_2^*$, and $\psi^*$. For regions in which the gradient of the value function is continuous, the optimal strategies must satisfy two conditions, which are often referred to as Isaacs Conditions. The regions in which the value function or its gradient is discontinuous are called singular surfaces and will be discussed in a later section.

*Theorem 1:* Suppose that the value function and the value function gradient are continuous. The control strategies for the three agents are then given by

Optimal Control Strategy of $E_1$:

$$\cos\theta_1^* = \frac{\lambda_1}{\rho_1} \qquad \sin\theta_1^* = -\frac{\lambda_\alpha}{d_1 \rho_1}$$

$$\rho_1 = \sqrt{\lambda_1^2 + (\tfrac{\lambda_\alpha}{d_1})^2} \tag{41}$$

Optimal Control Strategy of $E_2$:

$$\cos\theta_2^* = \frac{\lambda_2}{\rho_2} \qquad \sin\theta_2^* = \frac{\lambda_\alpha}{d_2 \rho_2}$$

$$\rho_2 = \sqrt{\lambda_2^2 + (\tfrac{\lambda_\alpha}{d_2})^2} \tag{42}$$

Optimal Control Strategy of P:

$$\cos\psi^* = -\frac{c_1}{\rho_p} \qquad \sin\psi^* = -\frac{c_2}{\rho_p}$$

$$\rho_p = \sqrt{c_1^2 + c_2^2} \tag{43}$$

where

$$c_1 = \tfrac{\lambda_\alpha}{d_2}\sin\alpha - \lambda_1 - \lambda_2\cos\alpha \tag{44}$$

$$c_2 = \tfrac{\lambda_\alpha}{d_1} - \lambda_2\sin\alpha - \tfrac{\lambda_\alpha}{d_2}\cos\alpha \tag{45}$$

The proof of this theorem is omitted to satisfy space constraints, but it can be found in the extended version of this paper.

### *B. Numerical Analysis*

Finding an analytic solution to the optimal trajectories is not practical due to the nonlinear and coupled nature of the state and adjoint equations. In order to numerically generate the optimal trajectories, we first substitute the optimal control strategies (41)-(43) into the the kinematic equations (7)-(11) and the adjoint equations (25)-(30). The resulting system of twelve ordinary differential equations describe the optimal trajectories of the three agents and the corresponding costates for this game. We can then numerically integrate backwards in time from the terminal surface to generate the optimal trajectories.

To find the initial conditions for integration we consider a point on the terminal surface:

$$\mathbf{x}_f = (\ d_{1f},\ d_{2f},\ \alpha_f,\ \beta_f,\ x_f,\ y_f\ )^T \tag{46}$$

where $d_{1f} = d_c$ and $d_{2f} > d_c$. From (34)-(38), we find the terminal adjoint vector:

$$\lambda_f = (\ \nu_8(d_2 - d_c), 0,\ 0,\ 0,\ 0,\ 0\ \ )^T \tag{47}$$

After substituting the optimal control strategies into the Hamiltonian and evaluating at the terminal state, we may solve directly for $\lambda_{1f}$:

$$|\lambda_{1f}| = \tfrac{C_E(\mathbf{x}_f) + ct}{v_p - 1} \tag{48}$$

Knowing that $E_1$ attempts to delay capture by increasing $\dot{d}_1$, we use the positive value for $\lambda_1$. It should be noted that on the portion of the terminal surface that represents the capture of $E_1$, the terminal control for $E_2$ is undefined at the moment of capture. Conceptually this makes sense because $E_2$ can do nothing to further delay capture of $E_1$, and any change it can produce in $C_E$ will have no effect on the integral cost because the game has ended. But in order to perform the numerical integration, it is necessary to know the control for $E_2$ to start the numerical integration. For this purpose we can use the

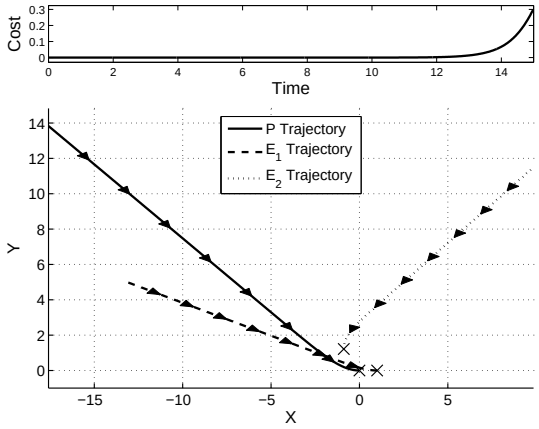


Fig. 2. Optimal Trajectories for $d_{2f} = 1.5$, $\alpha_f = 2.2$, and $v_p = 1.5$

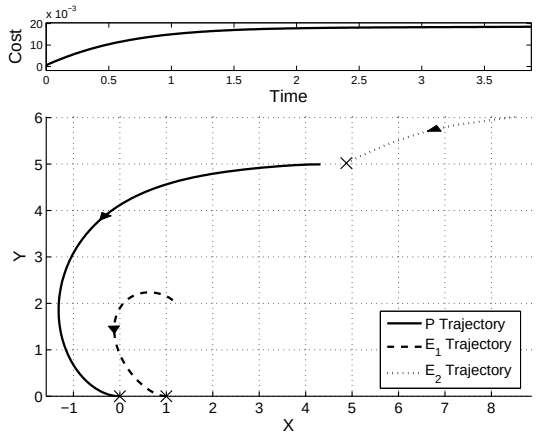


Fig. 3. Optimal Trajectories for $d_{2f} = 7$, $\alpha_f = .8$, and $v_p = 2.5$

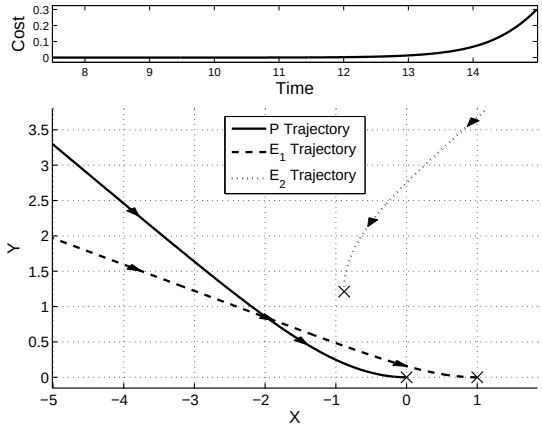


Fig. 4. Enlarged View of Near Capture Trajectories of Fig. 2

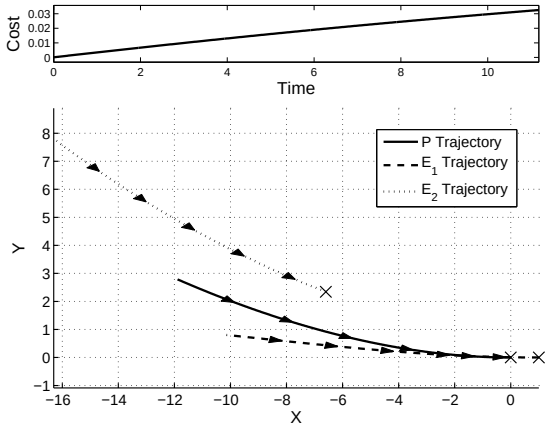


Fig. 5. Optimal Trajectories for $d_{2f} = 7$, $\alpha_f = 2.8$, and $v_p = 1.1$

control just before capture, which can be found by taking the limit:

$$\lim_{t\to t_f} \tan\theta_2 = \lim_{t\to t_f} \frac{\lambda_\alpha}{d_2\lambda_2} = \lim_{t\to t_f} \frac{\dot{\lambda}_\alpha}{d_2\dot{\lambda}_2 + \dot{d}_2\lambda_2} = \frac{\dot{\lambda}_\alpha(t_f)}{d_{2f}\dot{\lambda}_2(t_f)} \qquad (49)$$

We can now use the given terminal state $\mathbf{x}_f$ (46), terminal values found for $\boldsymbol{\lambda}_f$ (47), and the terminal control for $E_2$ (49) as initial conditions for our backwards in time numerical integration. The state equations are then integrated over the time period of interest or until the trajectory reaches a dispersal surface.

### C. Illustrative Cases

After the integration is performed, the resulting trajectories in the reduced coordinate system can then be mapped to trajectories in the global coordinate system using (2)-(4). Several illustrative cases are displayed in Fig. 2 through Fig. 5. In each of these figures, the solid line represents the trajectory of the pursuer; the dashed line represents the trajectory of $E_1$; and the dotted line represents the trajectory of $E_2$. In all three cases, the game is terminated when $E_1$ is captured. The terminal position of the three agents are marked by an x. The markers along the curves represent the agent locations in two second increments. In Fig. 2, $E_2$ rushes to meet near the point of capture in order to perform a last ditch flanking maneuver and create a large accumulation of cost just before capture. This results in a counter flanking maneuver by the pursuer just before capture. An enlarged view of the trajectories just before capture can be seen in Fig. 4.

In Fig. 3, the pursuer utilizes its speed advantage and performs a counter flanking maneuver against the two evaders in order to minimize the evader generated cost. In this scenario, $E_1$ can increase the cost to the pursuer more by attempting to remain close and flanking as opposed to a strategy of maximizing the time of the game by fleeing. This is similar to a fight or flight decision in nature. $E_1$ knows that it presents more of a cost to the pursuer by making a stand, and the evaders hope that this cost may be more than the pursuer is willing to accept and therefore aborts the attack. Although the initial conditions of this scenario shown in Fig. 5 are similar to Fig. 3, the pursuer does not possess the same speed advantage. Therefore, it does not try to outflank the evaders and instead takes a more direct approach towards $E_1$. Also, $E_1$ can accumulate more cost by running away and dragging the game out for a longer period of time. Again, this is a fight or flight situation, but it is more advantageous for $E_1$ to flee. Throughout the game, $E_2$ continues to harass the

pursuer from behind and accumulate cost.

### D. Singular Surfaces

The value function generated by the optimal control strategies divides the state space into mutually disjoint regions. Within these regions, the value function is well defined by the optimality conditions. The manifolds that divide these regions are called singular surfaces and are characterized by at least one of the following three characteristics: the optimal control strategies are not uniquely determined by optimality conditions previously described, the value function is not continuously differentiable, or the value function is discontinuous [16]. Most singular surfaces are not identified by backward integration of the optimal trajectories and require further analysis in order to describe the system behavior on or near these surfaces.

Within this game, symmetry in the kinematic equations and cost function hint at the existence of particular singular surfaces. We will begin our analysis of the singular surfaces by looking at the $\alpha = 0$ plane. On this plane, the three agents are in a collinear configuration with both evaders on one side of the pursuer. The pursuer can then direct its beam of focus at both evaders simultaneously, thereby completely negating the evader-generated cost. As a result, the pursuer would like to keep the state near the $\alpha = 0$ plane while the evaders attempt to force the state away from this plane. For the case where $c_t > 0$, the $\alpha = 0$ plane represents a dispersal surface. A dispersal surface is a surface within state space in which one or both of the players can select from multiple optimal control strategies. Each of these strategies moves the state off of the surface in different directions, but will result in the same value for the game. In this paper, for any game that begins with the initial state on the $\alpha = 0$ plane, the evaders make an initial choice to force the $\alpha$-component of the state away from zero in either the positive or negative direction. Either direction results in the same value of the game because of the symmetry of the state equations, cost function, and the resulting adjoint equations. Although the pursuer could attempt to hold the state near the $\alpha = 0$ plane, the slight reduction of evader-generated cost would be out weighed by the increased time penalty. This dispersal surface appears as a discontinuity of the gradient of the value function in the alpha-direction.

The $d_1 = d_2$ plane is also singular surface. The portion of this plane where $\alpha > \frac{\pi}{2}$ is clearly a dispersal surface where the pursuer chooses an evader to capture and forces the state off of the plane in that direction. Under certain conditions, the region of the $d_1 = d_2$ plane near the intersection with the $\alpha = 0$ plane has the potential for a singular focal surface. In this paper, we only consider initial starting positions above $\alpha = \frac{\pi}{2}$ on the $d_1 = d_2$ plane.

## IV. Conclusions

This paper has developed a novel single-pursuer, two-evader pursuit evasion game with an integral cost functional. In this game, the pursuer strives to minimize the total integral cost over the course of the game. The two-evaders are represented as a single player with two control variables and attempt to maximize the pursuer's cost. The generated optimal trajectories show that the proposed cost function generates cooperative defensive behaviors between the two evaders. These behaviors are similar to defensive grouping and predator mobbing found in nature and could be used in groups of unmanned systems in order to make attack a less appealing option for an opposing force.

Future work consists of assigning a cost threshold in which the pursuer would elect not to attack. We could then define a region in state space for which pursuit would be too costly. We would also like generalize the system to work for an arbitrary number of evaders. Although the evader generated cost can easily be extended to account for more agents, the new evaders would create many more singular surfaces that would greatly increase the complexity of the game and require further analysis.

## References


[1] R. Olendorf, T. Getty, and K. Scribner, "Cooperative nest defence in red-winged blackbirds: reciprocal altruism, kinship or by-product mutualism?" *Proceedings of the Royal Society of London Series B-Biological Sciences*, vol. 271, no. 1535, pp. 177–182, 2004.

[2] B. GRAW and M. MANSER, "The function of mobbing in cooperative meerkats," *Animal Behaviour*, vol. 74, no. 3, pp. 507–517, 2007.

[3] D. P. Croft, R. James, P. O. R. Thomas, C. Hathaway, D. Mawdsley, K. N. Laland, and J. Krause, "Social structure and co-operative interactions in a wild population of guppies (Poecilia reticulata)," *Behavioral Ecology and Sociobiology*, vol. 59, no. 5, pp. 644–650, 2005.

[4] L. Dugatkin, *Cheating monkeys and citizen bees: the nature of cooperation in animals and humans.* Simon and Shuster, 1999.

[5] L. Dugatkin, M. Mesterton-Gibbons, and A. Houston, "Beyond The Prisoners-Dilemma - Toward Models to Discriminate Among Mechanisms of Cooperation In Nature," *Trends in Ecology & Evolution*, vol. 7, no. 6, pp. 202–205, 1992.

[6] M. Mesterton-Gibbons and T. N. Sherratt, "Neighbor intervention: a game-theoretic model." *Journal of theoretical biology*, vol. 256, no. 2, pp. 263–75, 2009.

[7] R. Isaacs, *Differential Games*. New York: Wiley, 1965.

[8] S. Bhattacharya, S. Hutchinson, and T. Basar, "Game-theoretic analysis of a visibility based pursuit-evasion game in the presence of obstacles," in *2009 American Control Conference*. IEEE, 2009, pp. 373–378.

[9] M. Pontani and B. A. Conway, "Optimal Interception of Evasive Missile Warheads: Numerical Solution of the Differential Game," *Journal of Guidance, Control, and Dynamics*, vol. 31, no. 4, pp. 1111–1122, 2008.

[10] ——, "Numerical Solution of the Three-Dimensional Orbital Pursuit-Evasion Game," *Journal of Guidance, Control, and Dynamics*, vol. 32, no. 2, pp. 474–487, 2009.

[11] R. R. Brooks, J.-E. Pang, and C. Griffin, "Game and Information Theory Analysis of Electronic Countermeasures in Pursuit-Evasion Games," *IEEE Transactions on Systems, Man, and Cybernetics - Part A: Systems and Humans*, vol. 38, no. 6, pp. 1281–1294, 2008.

[12] S. D. Bopardikar, F. Bullo, and J. A. P. Hespanha, "On Discrete-Time Pursuit-Evasion Games With Sensing Limitations," *IEEE Transactions on Robotics*, vol. 24, no. 6, pp. 1429–1439, 2008.

[13] J. V. Breakwell and P. Hagedorn, "Point capture of two evaders in succession," *Journal of Optimization Theory and Applications*, vol. 27, no. 1, pp. 89–97, January 1979.

[14] W. Getz, "2-Target Pursuit-Evasion Differential-Games in the Plane," *Journal of Optimization Theory and Applications*, vol. 34, no. 3, pp. 383–403, 1981.

[15] A. Merz, "To Pursue or to Evade - That is the Question," *Journal of Guidance, Control, and Dynamics*, vol. 8, no. 2, pp. 161–166, 1985.

[16] T. Basar and G. J. Olsder, *Dynamic Noncooperative Game Theory*, 2nd ed. Philadelphia: Society for Industrial and Applied Mathematics, 1999.

# In-Flight Dynamically Adaptive Configurations: Lessons from Live Lepidoptera

Animesh Chakravarthy* and Roberto Albertani †
*University of Florida-REEF, Shalimar, FL 32548, USA*
and Johnny Evers‡
*Air Force Research Laboratory/RWGI, Eglin AFB, FL 32542, USA*

**This paper discusses the collection, post-processing and subsequent evaluation of flight data of butterflies, in various free flight scenarios. A vision tracking system is used to obtain the flight data; and this in turn is used to determine estimates of the motion of different body parts of the insect, including the abdomen and the wings. These estimates are subsequently analyzed with a view to establishing the manner in which the insect adapts the motion of its abdomen to work in tandem with the motion of its wings. Furthermore, the manner in which this adaptation changes through different flight phases is studied.**

## I. INTRODUCTION

The aerospace engineering community is increasingly interested in the flight mechanics and dynamics of small flapping air vehicles, Figure 1(a), and natural organisms in the low Reynolds number regime. The

**Figure 1. (a) A 20 cm wingspan ornithopter with a flexible wing in the REEF small wind tunnel. (b) The rain forest at the McGuire Center for Lepidoptera and Biodiversity, Gainesville, FL.**

observation and study of flying animals offers a significant source of bio-inspiration in several aeronautical disciplines including highly dynamic adaptive structures. While flight measurements of biological systems are relatively abundant, a meaningful recording of the data and an efficient distillation of their results is a work-in-progress endeavor. Comprehensive data on insects flying in their natural environments are extremely rare.

*Research Assistant Scientist, Dept. of Mechanical and Aerospace Engineering, and AIAA Senior Member.
†Research Assistant Professor, Dept. of Mechanical and Aerospace Engineering, and AIAA Senior Member.
‡Senior Engineer, Air Force Research Laboratory, RWGN, Eglin AFB, and AIAA Associate Fellow.

This paper presents the experimental techniques used for collecting live flight data from Lepidoptera in their natural environment and illustrates results on their significant capabilities to adapt their intricate wings-abdomen-thorax system to a variety of flight conditions including some extremely aggressive non-steady maneuvers.

The flight measurements were performed at the Butterfly Rainforest at the McGuire Center for Lepidoptera and Biodiversity, Figure 1(b), which is a 650 square meter screened vivarium at the Florida Museum of Natural History in Gainesville, FL. This center houses over 460 species of subtropical and tropical plants and trees to support up to $2,000$ free-flying butterflies of 120 different species. Natural fliers demonstrate a diverse array of flight capabilities, many of which are poorly understood. NASA established a research project to explore and develop flight technologies inspired by biological systems.[1] Aerodynamic research on flapping insect wings revealed mechanisms such as leading edge vortices (LEVs) and offered design criteria for insect-based flying machines.[2]

There have been numerous research projects performed by the biology community on the flight and structural behavior of insects. Significant research was performed presenting measurements of insects flight data considering the specimen as a multi-body system including head and thorax. For example, in the Calliphora vicina (Blowfly) it was shown that there exists a high level of correlation between the head and thorax movements; these were measured using sensor coils and during the insect's saccades angular rates of a few thousands of degrees per second were observed.[3] A relevant contribution of the abdomen posture on flight control mechanisms was presented in the male of Schistocerca gregaria (Male desert locust) suggesting that the sensory cue evoking the yaw response is a change in the direction of the relative wind, monitored by the cephalic wind receptor hairs.[4] The adaptability of the Lepidoptera to different flight requirements was observed by a non-symmetric passive wing twisting during upstroke and downstroke in the Insecta Papilionoidea[5] and during the highly un-steady take-off phase in the Pieris melete.[6] Using the evolution of neotropical butterflies as a natural experiment, a correlation between body center of gravity position and flight maneuverability was demonstrated focusing on the relative proportions of the thorax and abdomen as well as the palatability characteristics of different species of butterflies.[7] Flight data gathered during previous work on Idea Leuconoe (Tree Nymph) showed an apparently significant abdomen activity in certain flying phases with a significant correlation with the flapping wing and body dynamics.[8]

There has also been prior work done on locusts tethered in a wind tunnel with the objective of studying their longitudinal flight dynamics.[10–12] Force measurements are obtained in the wind tunnel, which are then used to determine stability derivatives of the insect under different relative wind velocities and angles of attack. The literature also comprises of a discussion on the use of CFD based modeling for the purpose of studying insect aerodynamics and flight dynamics.[13] This paper, on the other hand, relies on free flight data - an advantage of this is the ability to study different maneuvering flight phases of the insect; this advantage however is usually tempered by the fact that the accuracy of wind tunnel data is often better than that of free flight data. This work is aimed at determining the mechanisms used by live butterflies at adapting their intricate abdomen and elastic wings system to non-steady flight conditions. These approaches could lead to the development of new flight mechanics strategies for micro and nano air vehicles.

## II. The Experimental Set Up and Post Processing

The design of the data acquisition system (DAQ) was based on two key requirements: being non-obtrusive and having the capability of field measurements, i.e. allowing measurements in the insects' natural environment. A vision-based estimation method is used to study the insect flight with insignificant interference with the natural behavior of the insects. The visual system is composed of two high-speed digital cameras synchronized as a stereo pair, as schematically illustrated in Figure 2(a). A stereo pair of cameras with known parameters and relative pose allows estimation of 3D position of points in space. The measurements were performed under natural sunlight conditions at $100 - 200$ frames per second and resolutions of $800x600$ pixels. Figure 2(b) shows the cameras and computer hardware at their experimental location.

A sequence of pictures of the desired event is captured from both cameras and converted to two videos, one for each camera, using a combination of custom and commercial software. The videos are digitized using a stereoscopy tracking software[15] and accurate camera calibration data in order to perform 3D stereovision estimation of selected points on the target. The tracking software employed uses a 11-point Direct Linear Transformation (DLT) method for calibration.[14] The validation of the data acquisition and post processing methodology, including an estimation of the uncertainties was achieved by using a custom made target

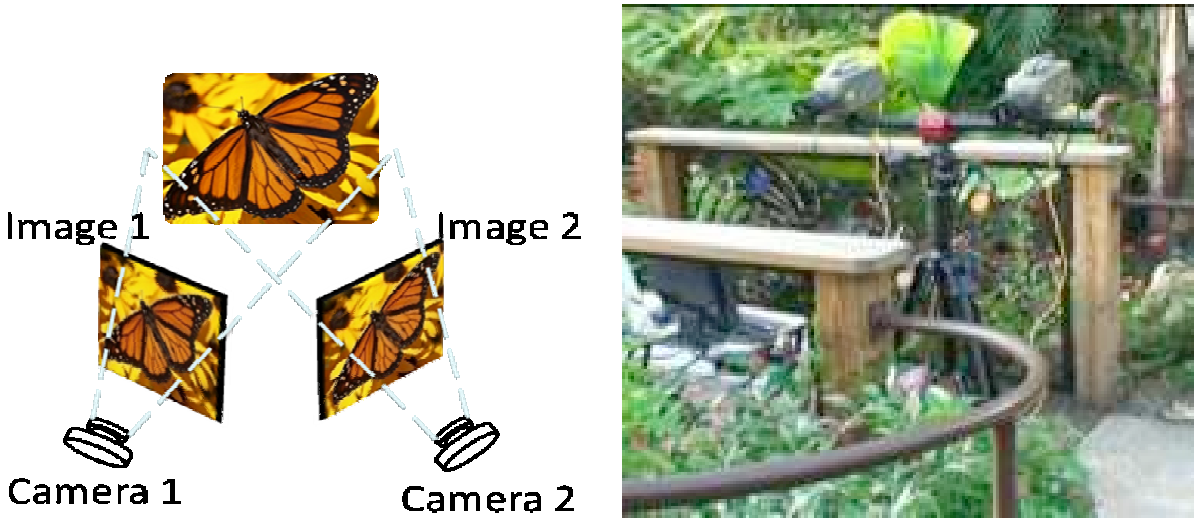


**Figure 2. (a) The stereo triangulation technique used by the cameras. (b) The stereo cameras in the experimental environment.**

consisting of multiple spring-mass components mounted on a shaker. The target has three parts simulating a body, a head and an antenna; and the shaker is controlled by a computer which can induce any desired oscillatory motion to the body. The targets three-dimensional position in time was measured using a high resolution dynamic visual image correlation (VIC) normally used in experimental mechanics.[9] Comparisons with the positions acquired by the tracking software selected for the measurements on butterflies provide estimates of the experimental uncertainties. A sample frame from a video is illustrated in Figure 3, describing an Idea Leuconoe (Tree Nymph) butterfly during an approach for landing on a leaf. In this case a total of four points including the tips of the left and right wings, the tip of the abdomen and the abdomen root, were tracked.


**Figure 3. Tracking of body parts of a butterfly during natural flight. Note the tracked points on the wing tips and the abdomen.**

The raw data may contain substantial voids due to points on the target being occluded, usually by other body parts or by foliage. Methods of statistical curve-fitting to fill in missing data are used and smooth time histories of the 3D position estimation are obtained, as depicted in Figure 4.

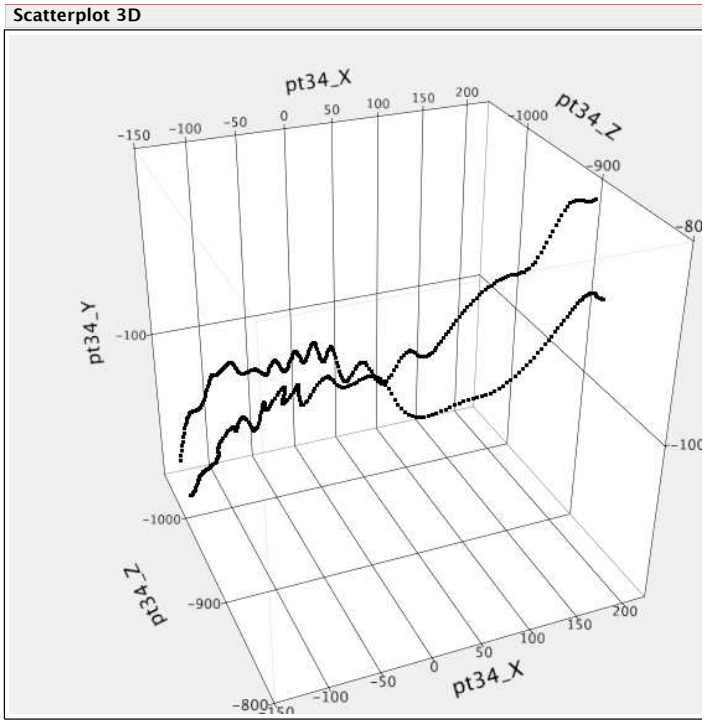


**Figure 4. Three-dimensional estimates of wing tips of a butterfly during natural descending flight. The trajectories are depicted after the smoothing process.**

## III. Results

Data obtained from the live measurements is the processed with several objectives in mind. The kinematics and dynamics of the butterflies' flight are the focus of the flight mechanics segment of the overall project. The shape-changing and relative elastic deformation of the various body parts, specifically the abdomen, the wings, the head and the antennae are the focus of the structural and aeroelastic segment. A combination of these two segments enables the investigation of possible correlations with the overall flight trajectory and performance of the insect. Three samples of the numerous flight events recorded in several sessions will be presented as examples of dynamic in-flight adaptation of the body-wings system.

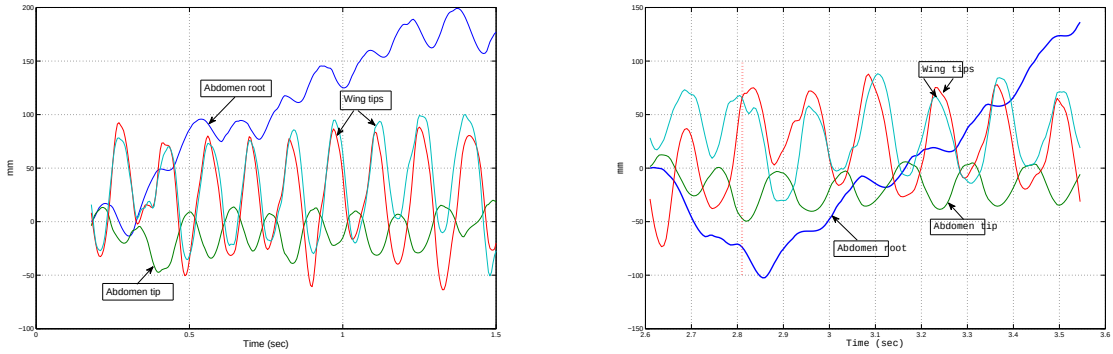


**Figure 5. Several flapping cycles of abdomen tip and wings demonstrated during a fly-by sequence**

Before we go into a more detailed study of the relative motion of the wings and abdomen in highly maneuvering flight, we briefly present a figure from a slightly benign flight sequence which is of a relatively long duration and that enables us to witness several flapping cycles. This is given in Figure 5, which shows

the vertical axis position of the wing tips and the abdomen tip relative to the abdomen root.

This figure clearly shows that for all the flapping cycles on display, the abdomen tip motion is nearly 180 deg out of phase with the wing tip motion. Also shown in the figure, is the vertical axis displacement of the abdomen root. In the particular flight sequence shown in Figure 5(a), the insect exhibited some periodicity in its overall flight trajectory, and interestingly the number of cycles of the abdomen root motion is exactly equal to the number of cycles of motion of each of the wing and the abdomen. Furthermore, Figure 5(a) demonstrates what appears to be a clear phase lag of the translational motion of the abdomen root (which represents the overall motion of the insect), relative to the wing and the abdomen tip motion; and this seems to indicate that the insect is using its abdomen as an active control device, at least during this particular flight phase.

The flight discussed above does not comprise of any significantly rapid maneuvers. We now turn our attention to a flight (of an insect from the same species) that does comprise a sequence of rapid maneuvers. More specifically, we now look at a flight that comprises of an acceleration phase, followed by a deceleration, followed by a turn and finally a phase of pure descent. During the 180 degree saccade on a horizontal plane with near zero turning radius the butterfly's abdomen adapts to the wing motion and significantly contributes to the dynamics of the turn. This 180 degree turn in yaw was performed in Flight 072708_0101 by an Idea leuconoe (Tree Nymph). A few snapshots of the flight are given in Figure 6.

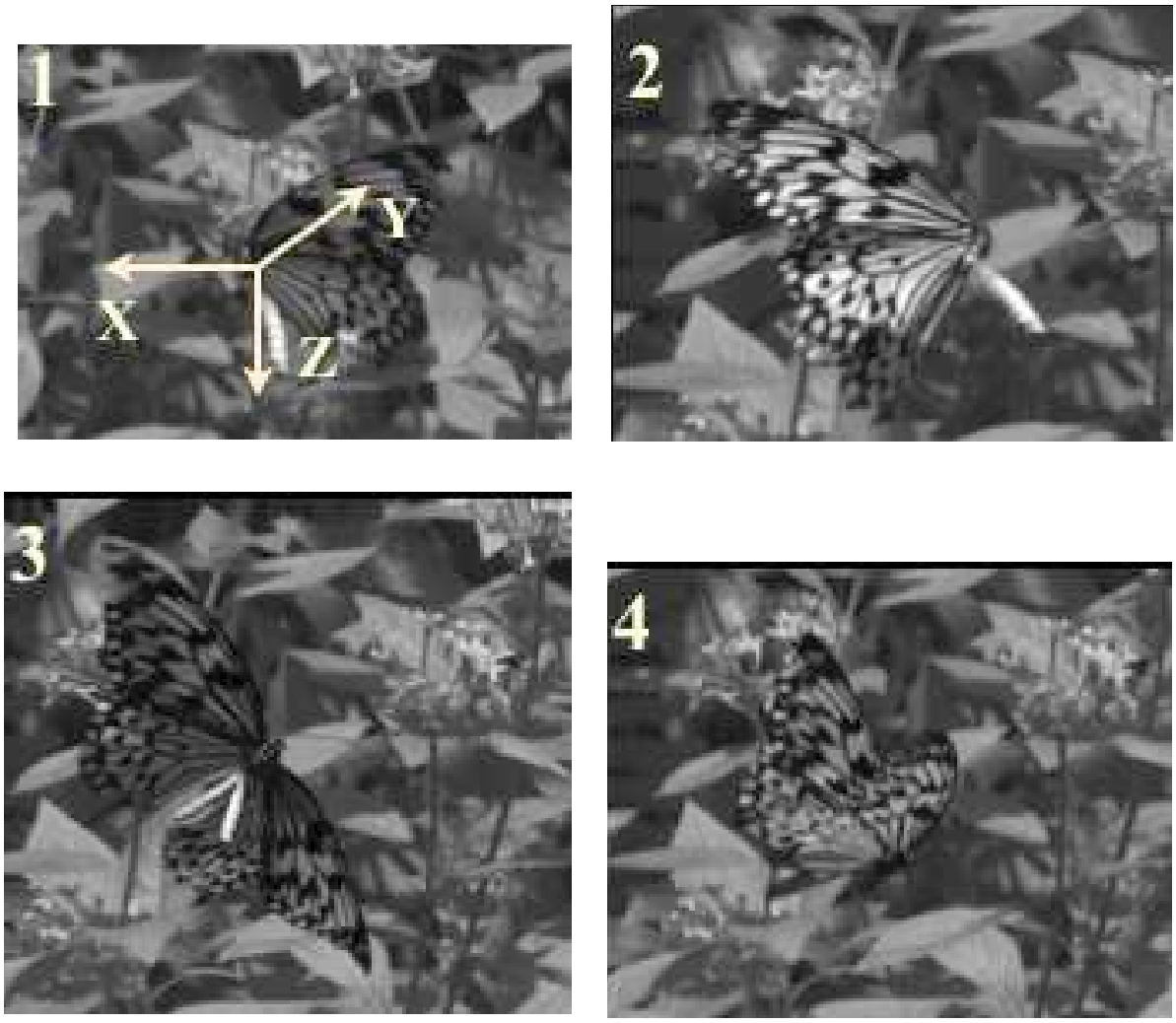


**Figure 6. Sequence during the Tree Nymph saccade. In (1) the butterfly starts a rapid deceleration with an aggressive yaw (2) and roll (3) motions. In (4) it starts a steady descent.**

The sequence of phases during this flight are as follows:

a) The insect initially accelerates in the forward direction, while reducing the y-axis component of its velocity to near zero. This is clearly brought out in Figure 7 which shows the insect velocity (which is represented by the velocity of the abdomen root). b) It then decelerates as it readies itself for a turn. In this phase, first the

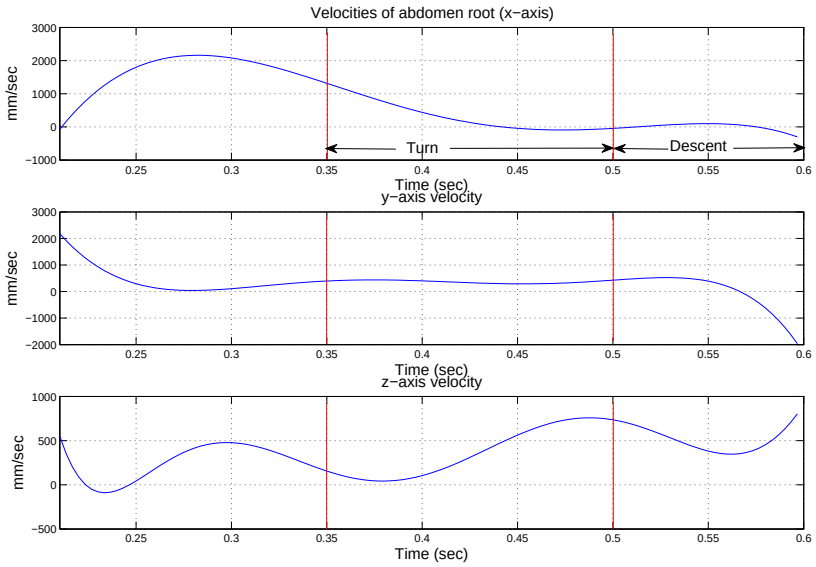


**Figure 7. Overall velocity of the insect**

forward velocity of abdomen root reduces till it comes down to zero. The abdomen tip however continues to move forward with some velocity. After about 0.1 sec, the forward velocity of abdomen tip too reduces to zero.

c) The head-thorax turns upwards, as the abdomen tip swings around, while the abdomen root performs a yawing turn. This is evident in Figure 8, which shows the trajectory of the abdomen root and the abdomen tip on a horizontal plane. In order to show the relative position of the abdomen root and tip during this trajectory, a line (dotted red) is also shown. One can thus see the motion of the abdomen root is initially curved as it takes a turn and then (its projection on the horizontal plane) moves along a straight line. The abdomen tip however continues to swing around even after the abdomen root has stopped its turn. The abdomen activity also seems to indicate that there is an adaptation of the insect mass-distribution for this small radius maneuver.

d) The wings typically flap in phase in symmetric flight although in this case, around this time, the wing tips are at 180 deg out of phase with each other, while the insect performs a roll. The fact that they become 180 deg out of phase is evidenced in Figure 9.

e) The insect loses altitude as the wing tips take some finite time to get back to flapping in phase with each other. The wing tips take about 0.1 sec to transition from 180 deg out of phase to back in phase. During that time interval, the insect loses close to 100 mm in altitude. All of these are evidenced in Figure 9.

f) As the two wings get back together in phase with one another, at the same time the abdomen tip gets itself back to 180 deg out of phase with the wings, which would represent the normal symmetric flying condition. This is also evidenced in Figure 9. At the beginning of the saccade the insect gives priority to the aerodynamic effects of the wings as well as positioning the abdomen vertically to maximize the drag. At the apex of the saccade the butterfly is using the abdomen inertia to execute a snap-roll and later to stabilize the flapping to go in a descending-hovering mode. The mass and inertia of the relatively heavy abdomen is dynamically adapted for the various phases of saccade. A relevant contribution to the gyration inertia management is also attributed to the wings' moving and closing at strategic times.

Figure 10 demonstrates the left wing tip and abdomen tip trajectories, shown on a vertical plane, relative to the moving abdomen root. The abdomen root is thus always at the origin of this figure. It is clearly seen that as the wing tip moves back and forth, as well as up and down, the abdomen tip too shows a back and forth and up and down motion. The starting points on each of the two curves are marked out

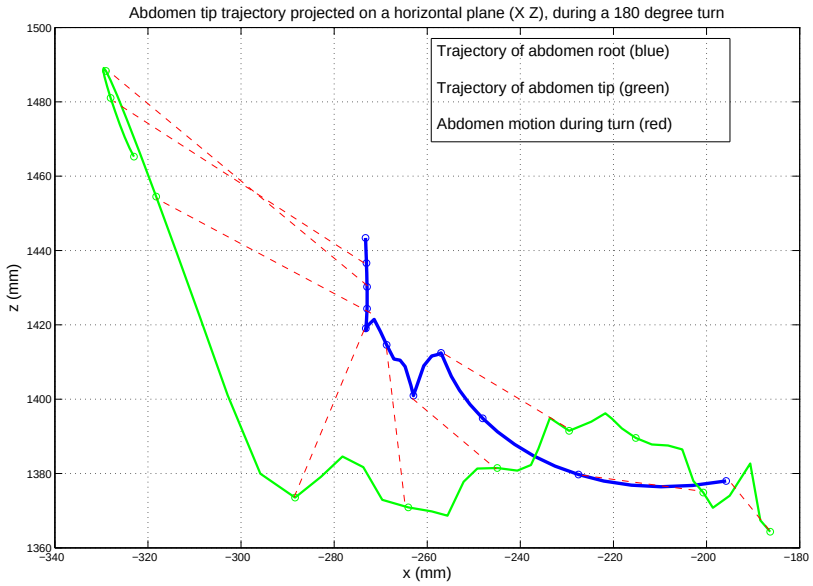


**Figure 8. Abdomen root and tip trajectory projected on a horizontal plane during a 180 degree turn.**

in small green circles. During the initial acceleration phase, the wing tip executes a stroke that is close to horizontal - this is in agreement with general intuition that horizontal wing strokes would be used for thrust generation. The abdomen tip stroke during this phase has both horizontal as well as vertical components. During the deceleration phase, the insect reduces its wing flapping speed and brings its wing tips high above the abdomen root. There is an accompanying twisting motion of the wings around this time (not visible on Figure 10), as the insect uses its wings as an airbrake of sorts to slow itself down. Simultaneously, it is seen that the insect brings its entire abdomen almost directly under the abdomen root and the horizontal stroke of the abdomen is very short during this phase. This is probably because the insect wants to sustain the abdomen in as close to a vertical position as possible since doing so can ensure that the abdomen contributes to the drag force. It then executes the turn, after which there is a phase of pure descent during which both the wing as well as the abdomen execute an almost vertical stroke.

Figure 10 thus demonstrates that the insect possesses significant abdomen motion to accompany the wing motion. In certain flight phases, such as the deceleration for instance, the role of the abdomen seems to complement that of the wing, as the insect uses both of them in a manner to increase the drag it experiences. In certain other flight phases, such as the turn, the abdomen seems to play a stronger role than the wings in generating the flight trajectory. For the data shown in Figure 10, we compute the flapping velocities of the wing tip and the abdomen tip. The components of these flapping velocities along the three inertial axes are shown in Figure 11(a). It is seen that during the initial acceleration phase, there is significant component of the flapping velocity along the X-axis, which is the direction of flight of the insect; and the same then reduces during the deceleration phase. The flapping velocity component of the abdomen, along the X-axis does not seem to be affected by the fact that the insect is accelerating or decelerating; but it does show the same periodicity as the wing and consistently remains in a phase opposite to that of the wing. During the turn, the X and Y axes flapping velocity components of the abdomen become almost comparable to that of the wing, thus indicating the strong role that the abdomen plays during a turn. Also, along the Y axes, the flapping velocity of the abdomen initially increases in phase with the wing, but this then gets disrupted till the occurrence of the turn, during which period, the abdomen tip velocity becomes nearly opposite in phase to that of the wing. Figure 11(b) then shows the X axis components of the flapping velocities of the wingtip and abdomen tip on a phase plane. The different flight phases are identified by different colors on this plot.

We can then take the scalar sums of the individual velocity components shown in Figure 11(a) to plot the flapping speeds of the wings and the abdomen. This is shown in Figure 12(a). In this figure, we see that the wing flapping speed is significantly higher than that of the abdomen in all phases of flight, except during the

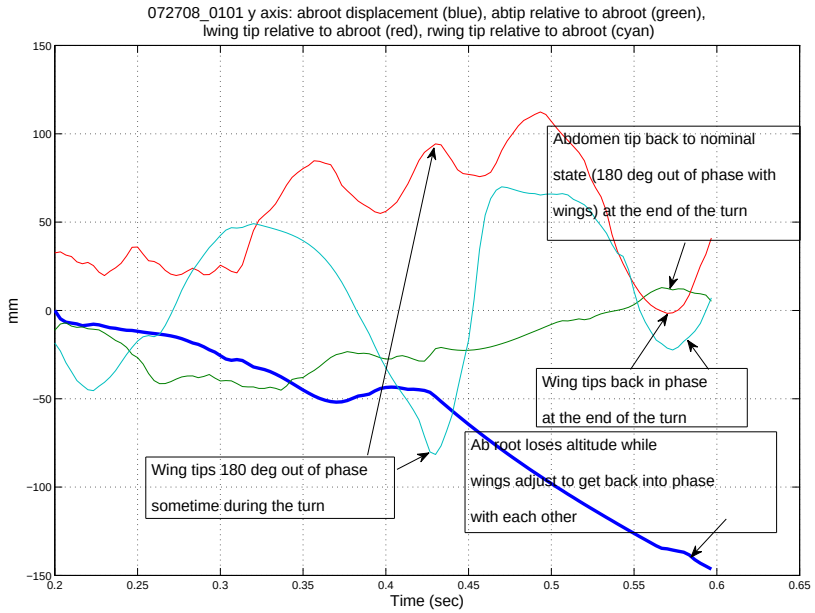


**Figure 9. Vertical axis trajectories of different body parts of the insect.**

turn. During the middle of the turn, the amplitude of the peak of the flapping speed is almost exactly equal to that of the wing. Yet by adjusting the relative phases of the two flapping speeds, the insect ensures that the ratio of abdomen tip flapping speed to the wing tip flapping speed is in excess of unity, during the turn. Note that during the initial acceleration and deceleration phases, the abdomen flapping speed varies almost in phase with the wing flapping speed; and it is just at the commencement of, and during the turn that this relative phase pattern gets disrupted. During the second half of the turn, there is an almost constant phase lag of the abdomen tip flapping speed in relation to the wing tip flapping speed. Figure 12(b) then shows the ratio of the abdomen tip flapping speed to the wingtip flapping speed during the different flight phases. It is clearly seen that this ratio becomes significantly high during the turn thus demonstrating the major role that the abdomen appears to play during the turning flight phase, at least as far as this particular ratio metric is concerned.

From the data of Figure 7 and assuming a nominal mass of 0.35 grams, we get the inertial forces acting on the insect. These are given in Figure 13, from which we see that the magnitudes of these forces are of the order of 0.01 Newtons. Figure 14(a) shows a comparison of the Reynolds Number of the wing tip and the abdomen tip through the different flight phases. For this computation, the characteristic length of the abdomen was taken as the abdomen length itself while for the wing, the characteristic length was taken as the mean aerodynamic chord of the wing. Typical values of these quantities for the species being considered are 0.02912 meters and 0.03844 meters, respectively. The diameter of the abdomen is typically 0.00485 meters. The Reynolds Number of the wing tip ranges from 2000 to about 15000, while that of the abdomen tip ranges from 2000 to about 8000. The Reynolds Number of the abdomen is generally lower than that of the wing, except during the acceleration and the turn phases. During these two phases, the Reynolds number of the abdomen tip is comparable to that of the wing tip. Figure 14(b) shows the advance ratio of the wing.

There is significant wing cambering activity as the butterfly prepares itself for the deceleration. This is demonstrated in Figure 15. To generate the plots in this figure, three representative points on the wing chord were tracked - one on the leading edge, a second on the trailing edge and a third in between the leading and trailing edges. In the frames when these three points are found to be nearly collinear, it is construed that there is negligible wing cambering, while at other times it is construed that there is significant wing camber. The wing cambering is demonstrated through a succession of frames, with the abdomen root being positioned at the origin of each of these Figures 15(a-d). In these figures, the color sequence is as follows: the first frame in each figure is represented in blue, followed by green, red, cyan and magneta. Also plotted

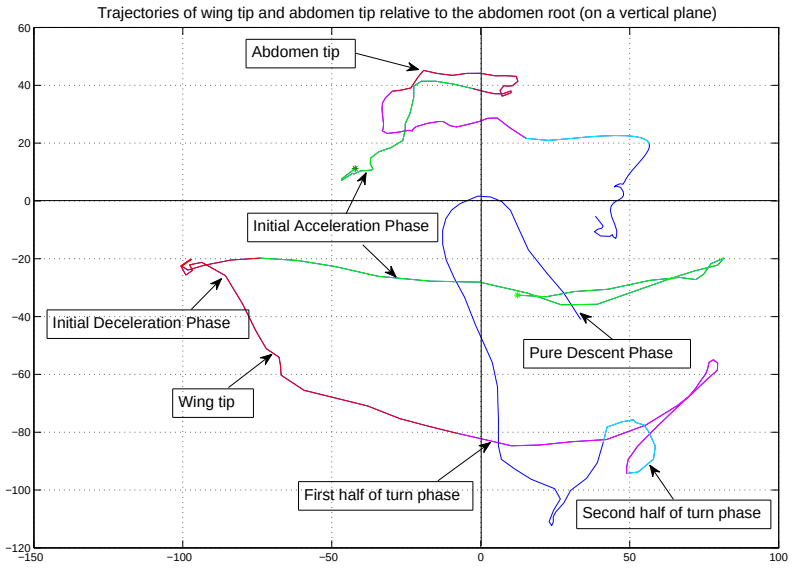


**Figure 10. Trajectories of left wing tip and abdomen tip shown relative to the abdomen root on a vertical plane. The different flight phases are identified by different colors.**

for the purposes of comparison, is the wing tip flapping velocity vector. From Figure 15(a), it is seen that in frame 66, the wing has negligible camber and then progressively gets cambered as it executes a downstroke. Figure 15(b) shows the continued presence of the camber during the wing upstroke motion. Some wing camber continues to be present further along the upstroke; and after the wing crosses the abdomen root, this camber then begins to reduce (as seen in Figure 15(c-d)).

The next relevant example of in-flight structural adaptation is presented with a glide flight with very mild flapping activity (flight number 0330080205). Interestingly enough the event displays an in-flight wings twisting and change of dihedral (on the single wing) with probably no inertia loads from flapping motion on the wing. This fact appears quite remarkable due to the absence of any muscles in the butterfly's wing. Figure 17 illustrates a three-dimensional plot of the trajectory of two chord-wise sections on each wing (right wing blue, left wing green). The absence of significant flapping and the presence of twisting activity are both evident. Again the abdomen (green line) is probably used to dynamically adapt the center-of-gravity position to the new flight requirements (the orientation changes at low rates).

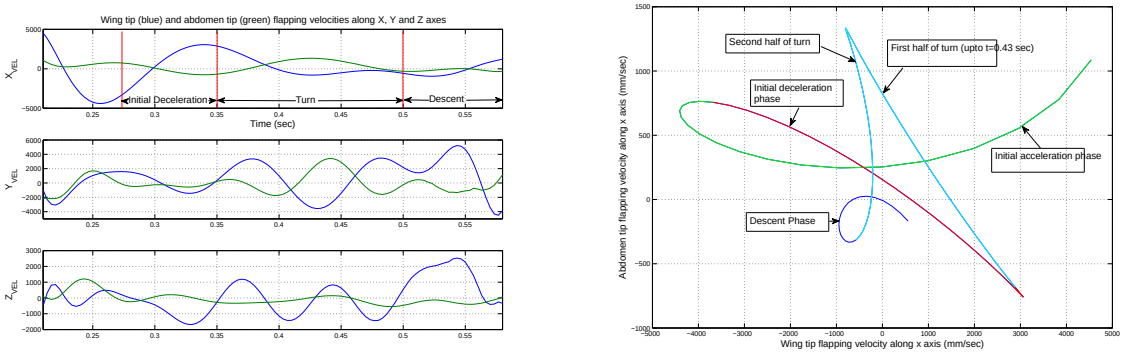


**Figure 11. (a) Wing tip and abdomen tip flapping velocities along the X,Y and Z axes. (b) Phase plane plot of wingtip and abdomen tip flapping velocities along the X axis.**

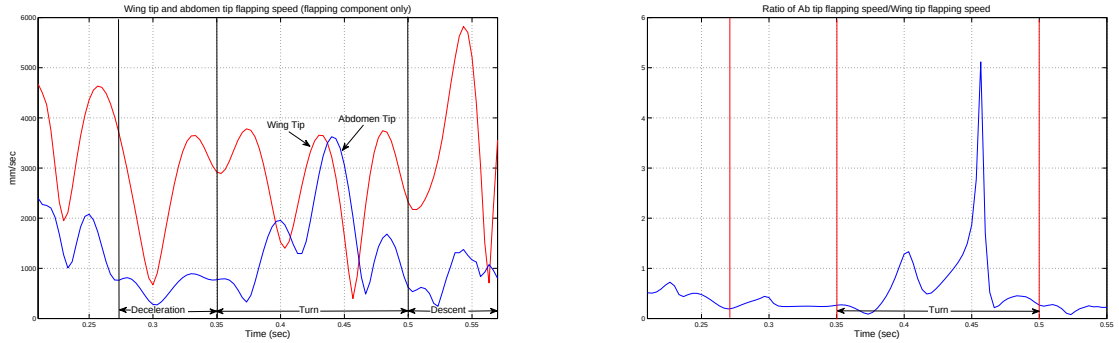


**Figure 12. (a) Comparison of wing tip and abdomen tip flapping velocities during different flight phases. (b) Ratio of abdomen tip flapping speed to wing tip flapping speed.**

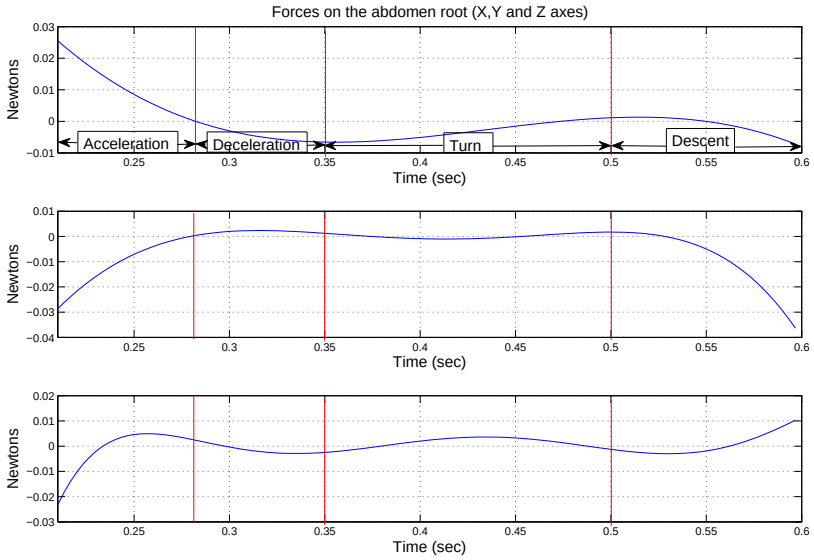


**Figure 13. Inertial force components on the insect**

## IV. Conclusions

This paper discusses the collection and analysis of free flight data of butterflies in their natural environment. A particular flight with several rapid changes in flight phase is evaluated, with the objective being to determine the manner in which the insect adapts the motion of its abdomen to that of its wings; and also to determine how the manner of this adaptation changes from one flight phase to the next. Instances of the insect adapting its wing shape in an aeroelastic manner are also demonstrated. Future work will comprise the use of sophisticated mathematical tools to perform a deeper analysis of this adaptive behavior.

## Acknowledgments

The authors would like to acknowledge the support from the Air Force Research Laboratory under contract F08635-03-D-0130, with Johnny Evers as project monitor. The authors would also like to acknowledge the logistical support from Dr. Thomas Emmel, Director of the McGuire Center for Lepidoptera and Biodiversity, Florida Museum of Natural History, University of Florida, Gainesville, and his staff towards obtaining the butterfly flight data; as well as Dr. Tyson Hedrick, Department of Biology at University of

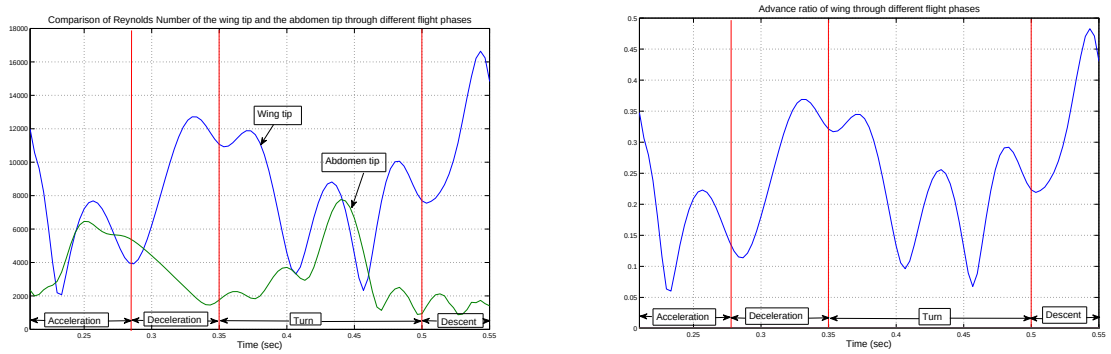


**Figure 14. (a) Comparison of Reynolds numbers of wing tip and abdomen tip through different flight phases. (b) Advance ratio of wing.**

North Carolina, for the use of his tracking software.

## References

[1]Raney, D., L., Waszak, M., R., "Biologically Inspired Micro-Flight Research," SAE 2003-01-3042.

[2]Ellington, C., P., "The Novel Aerodynamics of Insect Flight: Applications to Micro-Air-Vehicles," *The Journal of Experimental Biology*, 202, 3439-3448 (1999), The Company of Biologists Ltd 1999, JEB2214.

[3]Schilstra, C., Van Hateren, J., H., "Blofly Flight and Optical Flow I. Thorax Kinematics and Flight Dynamics," *The Journal of Experimental Biology*, 202, 1481-1490 (1999), The Company of Biologists Ltd 1999, JEB1989.

[4]Camhi, J., M., "Sensory Control of Abdomen Posture in Flying locusts," *Journal of Experimental Biology,* 52, 533-537, 1970, Printed in Great Britain, The Company of Biologists Ltd.

[5]Wootton, R., "Leading Edge Section and Asymmetric Twisting in the Wings of Flying Butterflies (Insecta Papilionoidea)," *The Journal of Experimental Biology*, 180, 105-117 (1993), Printed in Great Britain, The Company of Biologists Ltd.

[6]Sunada, S., Kawachi, K., Watanabe, I., Azuma, A., "Performance of a Butterfly in Take-Off Flight," *The Journal of Experimental Biology*, 183, 249-277 (1993), Printed in Great Britain, The Company of Biologists Ltd.

[7]Srygley, R. B., Dudley, R., "Correlations of the Position of Center Body Mass with Butterfly Escape Tactics," *The Journal of Experimental Biology*, 174, 155-166 (1993), Printed in Great Britain, The Company of Biologists Ltd.

[8]Chakravarthy, A., Albertani, R., Gans, N., Evers, J., "Experimental Kinematics and Dynamics of Butterflies in Natural Flight," *47th AIAA Aerospace Sciences Meeting*, Orlando, FL, 5-8 January, 2009.

[9]Albertani, R., Stanford, B., Hubner, J. P., and Ifju, P., "Aerodynamic Characterization and Deformation Measurements of a Flexible Wing Micro Air Vehicle," *SEM Journal*, DOI: 10.1007/s11340-006-9025-5.

[10]Taylor, G.K, Bomphrey, R.J, Hoen, J, "Insect flight dynamics and Control," *Aerospace Sciences Meeting and Exhibit*, AIAA 2006-32, Reno, 8-12 January 2006.

[11]Taylor, G.K, Zbiwoski, R, "Nonlinear time-periodic models of the longitudinal flight dynamics of desert locusts Schistocerca Gregaria," *Journal of the Royal Society Interface*, 2005(2), pp. 197-221.

[12]Taylor, G.K, Thomas, A.L.R, "Dynamic flight stability in the desert locust Schistocerca Gregaria," *Journal of Experimental Biology* 206, 2003, pp. 2803-2829.

[13]Zbiwoski, R, Ansari, S.A, Knowles, K, "On mathematical modelling of insect flight dynamics in the context of micro air vehicles," *Journal of Bioinspiration and Biomimetics*, Vol. 1, 2006, pp. R26-R37.

[14]"http://kwon3d.u-gm.com/theory/dlt/dlt.html"

[15]Hedrick, T., "Software techniques for two and three-dimensional kinematic measurements of biological and biomimetic systems," *Journal of Bioinspiration and Biomimetics*, Vol. 3, 2008.

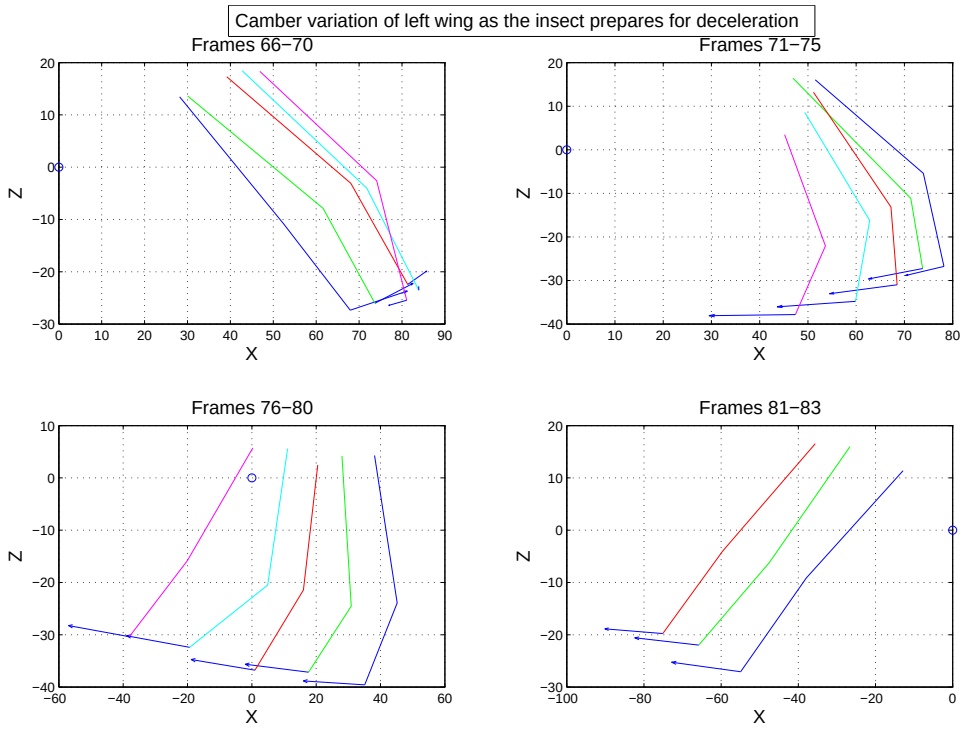


**Figure 15. Demonstration of wing cambering activity as the butterfly prepares for deceleration.**

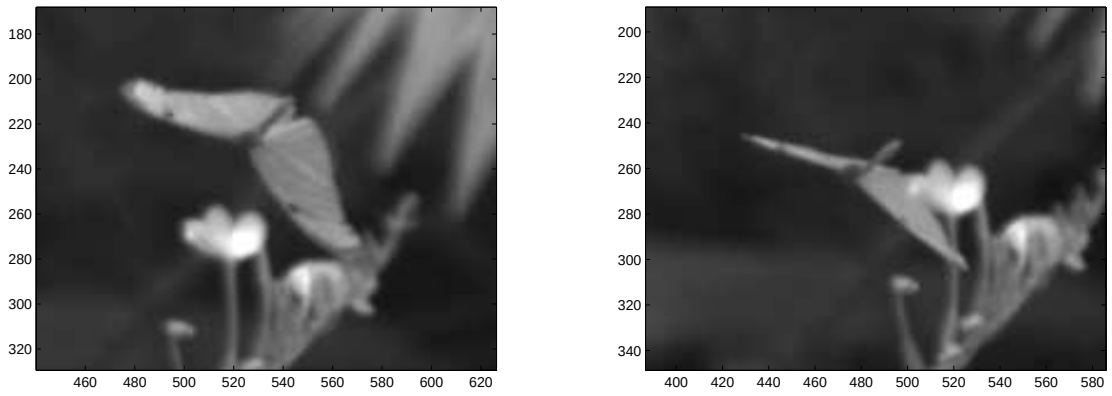

**Figure 16. (a) Snapshot frame demonstrating insect flight with wing dihedral. (b) Snapshot frame demonstrating insect flight with no wing dihedral.**

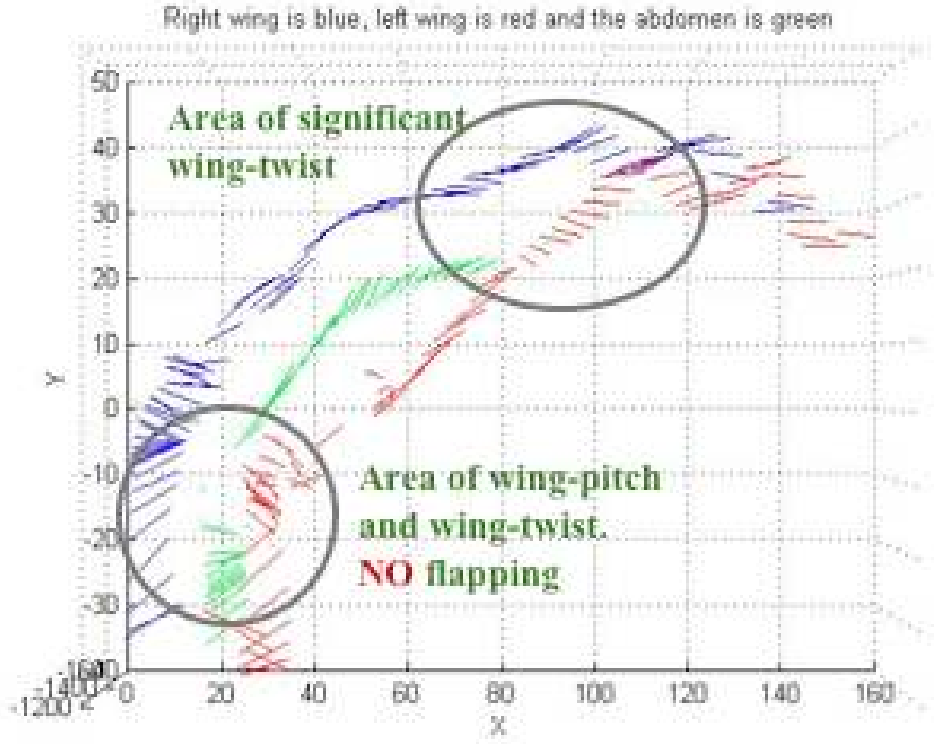


**Figure 17. Sequence during a steady descending glide with little flapping activity. The segments represent the right wing chord at mid-wing (blue), the left wing chord (red) and abdomen (green).**

# Sensitivities & Functional Gains for a Flexible Aircraft-Inspired Model

Animesh Chakravarthy, Katie A. Evans, and Johnny Evers

***Abstract*— Aeroelastic wing micro-autonomous aerial systems (MAAS) concepts are being explored for military and civilian applications. However, on the whole, the issues of control of MAAS are largely unexplored. Controllers designed using methods applicable to larger aircraft are unlikely to realize the agile flight potential of flexible wing MAAS airframes. In this paper, the authors use two Euler-Bernoulli beams connected to a rigid mass to model an aeroelastic wing MAAS. They employ Continuous Sensitivity Equation Methods to examine the sensitivity of the controlled state with respect to variation of the $H_\infty$ control parameter, with the primary goal being to gain insight into the flexible dynamics of the system in order to exploit the flexibility for control purposes. Further, the authors examine functional gains in order to determine optimal sensor placement while taking advantage of the flexibility of the MAAS model.**

## I. INTRODUCTION

Considerable work is currently underway to investigate the aerodynamics, structural dynamics, flight mechanics, and control associated with bio-inspired flight (see for example [1], [2], [3], [4], [5]). Consequently, aeroelastic wing micro-autonomous aerial systems (MAAS) concepts are being explored for military and civilian applications. Work from other projects (see for example [6], [7], [8], [9]) is laying the foundation required to eventually construct high fidelity dynamics models of MAAS, which do not currently exist, though key features of such models are emerging. However, on the whole the issues of control of agile aeroelastic wing MAAS are largely unexplored. All micro-scale vehicles developed to date exhibit only limited autonomy, generally way-point trajectory following, with limited agility.

In this paper, the authors use two Euler-Bernoulli beams connected to a rigid mass in an initial effort to model an aeroelastic wing MAAS. Each beam represents a flexible wing, while the rigid mass represents the fuselage. This "beam-mass-beam" model will be referred to as the BMB model system in this paper. The authors employ Continuous Sensitivity Equation Methods to examine the sensitivity of the controlled state with respect to variation of the $H_\infty$ control parameter, with the goal being to gain insight into the flexible dynamics of the system in order to exploit the flexibility for control design purposes. A secondary goal of this aspect of the research is to explore the possibility of determining an efficient assignment of the $H_\infty$ control parameter that is mathematically justified and does not require an iterative procedure for determination. Chen identified the problem of finding an optimal value for the control design parameter as an unsolved problem in systems and control theory [10]. Further, the authors examine both controller and observer functional gains in order to obtain insight into the problem of optimal actuator and sensor placement for MAAS systems. The approaches explored numerically in this paper seek to take advantage of the flexibility of aeroelastic wings and exploit the same to achieve agility as opposed to viewing this characteristic as a hindrance for control design.

The outline of the paper is as follows. The $H_\infty$ controller is summarized in Section II. Section III provides a description of the equations governing the partial differential equation (PDE) model, along with the variational forms of the PDE equations and state sensitivity. Numerical results are presented in Section IV. Conclusions and directions for future work are given in Section V.

## II. $H_\infty$ CONTROL DESIGN

In this section, the authors present a short overview of the $H_\infty$ compensator design in state space form [11], [12]. Assume the existence of a linear PDE system of the form

$$\dot{x}(t) = \mathscr{A}x(t) + \mathscr{B}u(t), \quad x(0) = x_0, \tag{1}$$

where $x(t) = x(t,\cdot) \in X$ is the state of the linear system and $X$ is a Hilbert space. Here, $\mathscr{A}$ is the system operator defined on $\mathbf{D}(\mathscr{A}) \subseteq X$ that, by assumption, generates an exponentially stable $C_0$ semigroup, $\mathscr{B}$ is the control operator, and $u(t)$ is the control input, defined on Hilbert space $U$, which is taken to be $\mathbb{R}^m$ in this work. It is assumed that knowledge of only part of the system can be obtained through the state measurement $y$ on Hilbert space $Y$, which is taken to be $\mathbb{R}^p$ in this work, where $y(t) = \mathscr{C}x(t)$. Assume an estimate of the state is used in the control law. To provide this estimate, a compensator is used that has the form

$$\dot{x}_c(t) = \mathscr{A}_c x_c(t) + \mathscr{F}y(t), \quad x_c(0) = x_{c_0} \tag{2}$$

and the feedback control law is written

$$u(t) = -\mathscr{K}x_c(t) \tag{3}$$

where $x_c(t) = x_c(t,\cdot) \in X$ is the state estimate. Designing a controller of this type requires determining $\mathscr{A}_c, \mathscr{F}$, and $\mathscr{K}$.

This work was supported by the Louisiana Board of Regents under Contract Number LEQSF(2007-10)-RD-A-21, the US Air Force Summer Faculty Fellowship Program, and the Air Force Research Laboratory under Contract Number FA8651-08-D-0108.

A. Chakravarthy is a Research Assistant Scientist of Mechanical and Aerospace Engineering, University of Florida, Research and Engineering Education Facility, 1350 N. Poquito Rd., Shalimar, FL 32579, USA animesh@reef.ufl.edu

K. Evans is with the Faculty of Mathematics and Statistics, P.O. Box 10348, Louisiana Tech University, Ruston, LA 71272, USA kevans@latech.edu

J. Evers is with the Air Force Research Laboratory, Munitions Directorate, 101 W. Eglin Blvd., Ste. 332, Eglin AFB, FL 32542 USA johnny.evers@eglin.af.mil

By solving the Riccati equations

$$\mathscr{A}^*\Pi+\Pi\mathscr{A}-\Pi(\mathscr{B}R^{-1}\mathscr{B}^*-\theta^2\mathscr{B}\mathscr{B}^*)\Pi+\mathscr{C}^*\mathscr{C}=0, \quad (4)$$

where $R:U\to U$ is a weighting operator for the control of the form $R=cI$, with $c$ a scalar and $I$ the identity operator, and

$$\mathscr{A}P+P\mathscr{A}^*-P(\mathscr{C}^*\mathscr{C}-\theta^2\mathscr{C}^*\mathscr{C})P+\mathscr{B}\mathscr{B}^*=0, \quad (5)$$

one can obtain the operators $\mathscr{K}$, $\mathscr{F}$, and $\mathscr{A}_c$ via

$$\begin{aligned}\mathscr{K} &= R^{-1}\mathscr{B}^*\Pi,\\ \mathscr{F} &= (I-\theta^2P\Pi)^{-1}P\mathscr{C}^*,\\ \mathscr{A}_c &= \mathscr{A}-\mathscr{B}\mathscr{K}-\mathscr{F}\mathscr{C}+\theta^2\mathscr{B}\mathscr{B}^*\Pi. \end{aligned} \quad (6)$$

The resulting feedback control is applied to the original linear system; the closed loop linear system is then defined by

$$\frac{d}{dt}\begin{bmatrix} x(t)\\ x_c(t)\end{bmatrix} = \begin{bmatrix}\mathscr{A} & -\mathscr{B}\mathscr{K}\\ \mathscr{F}\mathscr{C} & \mathscr{A}_c\end{bmatrix}\begin{bmatrix} x(t)\\ x_c(t)\end{bmatrix}. \quad (7)$$

For sufficiently small $\theta$, there are guaranteed minimal solutions $\Pi$ and $P$ to (4) and (5), respectively, such that $(I-\theta^2P\Pi)$ is positive definite and the linear closed loop system (7) is stable. Note that $\theta=0$ yields the classical Linear Quadratic Gaussian (LQG) compensator design. Since there exist no prescribed formulas for $\theta$, there is an inherent computational expense for this control design in choosing the parameter value. As a secondary goal, the authors seek to use sensitivity analysis to gain a better understanding of the $H_\infty$ controller. The goal is to develop a methodology for choosing $\theta$ to satisfy performance and robustness criteria, while justifying that choice based on the analysis. To this end, sensitivity analysis is applied to $H_\infty$ controlled distributed parameter systems to examine the sensitivity of the controlled state to $\theta$.

For certain PDEs, the control law in (3) can be written in integral form. That is,

$$u(t)=-\mathscr{K}x_c(t)=-\langle k_i(s),x_c(t)\rangle_X, \quad (8)$$

for spatial variable $s$ and where $k_i\in X$ for $i=1,2,...,m$ (see for example [13]), and the kernels of the integrals, $k_i(s)$, are called control functional gains. Control functional gains can be used to determine optimal sensor placement (see for example [14], [15], [16], [17]) because they provide information about the contribution of the state estimate to the overall controller. For example, an area where a control functional gain is large would indicate that area provides a state estimate value that contributes more significantly to the controller. Further, there would be potential benefit in placing sensors in that area.

Additionally, the observer gain operator $\mathscr{F}:\mathbb{R}^p\to X$ is continuous and has range in $\mathbf{D}(\mathscr{A})\subseteq X$. Then, for a state estimate of the form $x_c(t)=[w_c(t,\cdot)\ \ \frac{\partial}{\partial t}w_c(t,\cdot)]$, $\mathscr{F}$ has the representation

$$\mathscr{F}y=\begin{bmatrix} g_1(s) & \cdots & g_p(s)\\ h_1(s) & \cdots & h_p(s)\end{bmatrix}\begin{bmatrix} y_1\\ \vdots\\ y_p\end{bmatrix}\in X, \quad (9)$$

where $g_1(s),\ldots,g_p(s),h_1(s),\ldots,h_p(s)$ are called observer functional gains. To more completely analyze the problem of sensor placement, observer functional gains should be examined alongside control functional gains. For example, an area where an observer functional gain is large would indicate that area provides a measurement value of the state that contributes more significantly to the overall controller design. Thus, using similar logic applied in the case of control functional gains, there would be potential benefit in placing sensors in that area.

As documented in [14], this simple approach to sensor placement does not take into account issues such as performance and robustness. However, given the complex nature and relative lack of understanding of aeroelastic wing MAAS, it is reasonable to examine the functional gains in this problem as initial work toward the direction of designing sensors for these aircraft.

## III. AN AIRCRAFT-INSPIRED MODEL

In this work two Euler-Bernoulli beams connected on either side of a rigid mass are used to model an aeroelastic wing MAAS, hereafter referred to as the BMB system. The fuselage of the MAAS is assumed to be rigid. A schematic of the BMB system is given in Figure 1. Note that the BMB system is meant to represent primarily the heave dynamics of the MAAS. The MAAS is initially assumed to be flying with wings straight and level and in equilibrium with the lift balancing the weight. At time $t=0$, there is assumed to be a perturbation in the wings' shape (caused by a sudden gust, for example). This perturbed wing shape causes a change in the local angle of attack distribution over each wing and this in turn leads to a perturbation in the lift distribution denoted by $\Delta\text{Lift}(t,s)$. Each beam is modeled with both viscous and Kelvin-Voigt damping, and it is assumed that the material and inertial properties of both beams are homogenous and identical. Denoting the displacement of the left beam from its initial equilibrium position at time $t$ and position $s$ by $w_L(t,s)$ and the corresponding displacement of the right beam at time $t$ and position $s$ by $w_R(t,s)$, the model of the BMB system is described as follows:

$$\begin{aligned}&\rho a\frac{\partial^2}{\partial t^2}w_L(t,s)+EI\frac{\partial^4}{\partial s^4}w_L(t,s)+\gamma_1\frac{\partial}{\partial t}w_L(t,s)\\ &\quad+\gamma_2 I\frac{\partial^5}{\partial t\partial s^4}w_L(t,s)=\frac{-\Delta\text{Lift}(t,s)}{\ell/2}+b_L(s)u_L(t),\end{aligned} \quad (10)$$

for $0\le s\le \ell/2,\ t>0$, and

$$\begin{aligned}&\rho a\frac{\partial^2}{\partial t^2}w_R(t,s)+EI\frac{\partial^4}{\partial s^4}w_R(t,s)+\gamma_1\frac{\partial}{\partial t}w_R(t,s)\\ &\quad+\gamma_2 I\frac{\partial^5}{\partial t\partial s^4}w_R(t,s)=\frac{-\Delta\text{Lift}(t,s)}{\ell/2}+b_R(s)u_R(t),\end{aligned} \quad (11)$$

for $\ell/2 < s \leq \ell,\ t > 0$, subject to boundary conditions

$$
\begin{aligned}
&EI\frac{\partial^2}{\partial s^2}w_L(t,0) + \gamma_2 I\frac{\partial^3}{\partial t\partial s^2}w_L(t,0) = 0,\\
&EI\frac{\partial^3}{\partial s^3}w_L(t,0) + \gamma_2 I\frac{\partial^4}{\partial t\partial s^3}w_L(t,0) = 0,\\
&EI\frac{\partial^2}{\partial s^2}w_R(t,\ell) + \gamma_2 I\frac{\partial^3}{\partial t\partial s^2}w_R(t,\ell) = 0,\\
&EI\frac{\partial^3}{\partial s^3}w_R(t,\ell) + \gamma_2 I\frac{\partial^4}{\partial t\partial s^3}w_R(t,\ell) = 0,\\
&EI\frac{\partial^3}{\partial s^3}w_L(t,\ell/2) + \gamma_2 I\frac{\partial^4}{\partial t\partial s^3}w_L(t,\ell/2)\\
&-EI\frac{\partial^3}{\partial s^3}w_R(t,\ell/2) - \gamma_2 I\frac{\partial^4}{\partial t\partial s^3}w_R(t,\ell/2)\\
&\qquad = m\frac{\partial^2}{\partial t^2}w_L(t,\ell/2),\\
&w_L(t,\ell/2) = w_R(t,\ell/2),\\
&\frac{\partial}{\partial s}w_L(t,\ell/2) = \frac{\partial}{\partial s}w_R(t,\ell/2),\\
&EI\frac{\partial^2}{\partial s^2}w_L(t,\ell/2) + \gamma_2 I\frac{\partial^3}{\partial t\partial s^2}w_L(t,\ell/2)\\
&-EI\frac{\partial^2}{\partial s^2}w_R(t,\ell/2) - \gamma_2 I\frac{\partial^3}{\partial t\partial s^2}w_R(t,\ell/2)\\
&\qquad = I_z\frac{\partial^3}{\partial t^2\partial s}w_R(t,\ell/2),
\end{aligned}
\tag{12}
$$

where $\rho$ is the density of the beam material, $a$ is the cross-sectional area of the beam, $E$ is Young's modulus, $I$ is the area moment of inertia of the beam, $I_z$ is the mass moment of inertia of the rigid mass, $\gamma_1$ is the coefficient of viscous damping, $\gamma_2$ is the coefficient of Kelvin-Voigt damping, $m$ is the mass of the rigid connection between the beams, $b_L(s)$ is the control input function for the left beam, $u_L(t)$ is the controller for the left beam, $b_R(s)$ is the control input function for the right beam, $u_R(t)$ is the controller for the right beam, and $\Delta\text{Lift}(t,s)$ is the function representing the perturbed lift force on each of the beams. In this work, $I_z$ is taken to be zero, so the simulated BMB system is actually a free-free beam with a point load in the center.

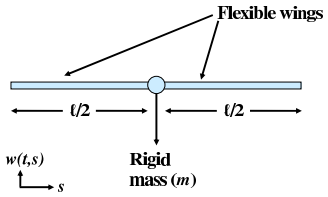


Fig. 1. MAAS model system.

Sensed information is used to design a feedback controller that regulates the MAAS model system to the exponentially stable zero equilibrium. It is assumed that the controllers act over the entire beam structures with control input functions of the form

$$b(s) = b_L(s) = b_R(s) = 0.5, \tag{13}$$

for $0 \leq s \leq \ell$, and available observations taking the form

$$y(t) = 0.25w(t,s), \tag{14}$$

for $0 \leq s \leq \ell$.

### A. Variational Form and Discretization of BMB System

Now consider the variational form of the BMB system in order to develop a Galerkin finite element approximation of the problem. For brevity, only the weak formulation of the left beam will be presented; the formulation for the right beam follows similarly. Employing the shorthand notation $\dot{w}(t,s) = \frac{\partial}{\partial t}w(t,s)$ and $w'(t,s) = \frac{\partial}{\partial s}w(t,s)$ for this discussion, the variational problem is that one seeks a $w_L(s) \in V = \{\varphi(\cdot) \in E\} \subset E = H^2(0,\ell/2)$ such that for all $\varphi \in V$

$$
\begin{aligned}
&\int_0^{\ell/2} \rho a\ddot{w}_L(t,s)\varphi(s)\ ds + \int_0^{\ell/2} EIw_L''''(t,s)\varphi(s)\ ds +\\
&\int_0^{\ell/2} \gamma_1\dot{w}_L(t,s)\varphi(s)\ ds + \int_0^{\ell/2} \gamma_2 I\dot{w}_L''''(t,s)\varphi(s)\ ds\\
&= \int_0^{\ell/2} \frac{-\Delta\text{Lift}(t,s)}{\ell/2}\varphi(s)\ ds + \int_0^{\ell/2} b_L(s)\varphi(s)u_L(t)\ ds.
\end{aligned}
\tag{15}
$$

Now choose a basis $\{b_i\}_{i=1}^N$ for the approximating space $V^N \subseteq V$, where $N$ corresponds to the number of gridpoints used in the finite element approximation. In particular, since $V^N \subseteq V \subset E = H^2(0,\ell/2)$, the state can be approximated by a linear combination of cubic splines. Then the state is approximated as

$$w_L(t,s) \approx w_L^N(t,s) = \sum_{i=1}^N c_i(t)b_i(s). \tag{16}$$

Using the state approximation (16) in (15) yields the matrix equation

$$M_0\ddot{c}(t) + D_0\dot{c}(t) + K_0c(t) = F_0(c(t)) + B_0u_L(t) \tag{17}$$

where $c(t) = [c_1(t),\ldots,c_N(t)]^T$, $M_0$ is the mass matrix, $D_0$ is the damping matrix, $K_0$ is the stiffness matrix, $F_0(c(t))$ contains the lift function, and $B_0$ is the input matrix, all defined by the following, for $i,j = 1,\ldots,N$:

$$
\begin{aligned}
[M_0]_{i,j} &= \int_0^{\ell/2} \rho a b_i(s)b_j(s)\ ds + mb_i(\ell/2)b_j(\ell/2)\\
&\quad - Ib_i'(\ell/2)b_j'(\ell/2),\\
[D_0]_{i,j} &= \int_0^{\ell/2} \gamma_1 b_i(s)b_j(s)\ ds\\
&\quad + \int_0^{\ell/2} \gamma_2 Ib_i''(s)b_j''(s)\ ds,\\
[K_0]_{i,j} &= \int_0^{\ell/2} EIb_i''(s)b_j''(s)\ ds,\\
[F_0(c(t))]_j &= \int_0^{\ell/2} \frac{-\Delta\text{Lift}(t,s)}{\ell/2}b_j(s)\ ds,\\
[B_0]_j &= \int_0^{\ell/2} b(s)b_j(s)\ ds.
\end{aligned}
\tag{18}
$$

Convert (17) into a first order system by defining $x_1(t) = c(t)$ and $x_2(t) = \dot{x}_1(t) = \dot{c}(t)$, thereby yielding

$$\begin{bmatrix} \dot{x}_1(t) \\ \dot{x}_2(t) \end{bmatrix} = \begin{bmatrix} 0 & I \\ -M_0^{-1}K_0 & -M_0^{-1}D_0 \end{bmatrix} \begin{bmatrix} x_1(t) \\ x_2(t) \end{bmatrix} + \begin{bmatrix} 0 \\ M_0^{-1}B_0 \end{bmatrix} u_L(t) + \begin{bmatrix} 0 \\ M_0^{-1}F_0(w(t)) \end{bmatrix}, \tag{19}$$

where $x = [x_1(t), x_2(t)]^T = \left[x_1(t), \frac{d}{dt}x_1(t)\right]^T$. Note that (19) is a finite-dimensional approximation of the system in (1).

### *B. Variational Form and Discretization of Sensitivity Equation for BMB System*

This framework now provides the basis for implementing control techniques discussed in Section II. Beyond control design, the authors are interested in examining the effects of the $H_\infty$ control parameter, $\theta$, on the displacement of the beams and the controller itself. The dependence of these quantities on $\theta$ is denoted explicitly with the following notation: $w_L(t,s) = w_L(t,s;\theta)$ and $u_L(t) = u_L(t;\theta)$, respectively. Continuous Sensitivity Equation Methods are employed for examining the sensitivities of these quantities to changes in the value of $\theta$ used in the $H_\infty$ control design. Make the following definitions for the sensitivities: $s_{w_L}(t,s;\theta) = \frac{\partial}{\partial\theta}w_L(t,s;\theta)$ for the sensitivity of beam displacement with respect to $\theta$ at time $t$ and spatial location $s$ and $s_{u_L}(t;\theta) = \frac{\partial}{\partial\theta}u_L(t;\theta)$ for the sensitivity of the controller with respect to $\theta$ at time $t$.

Now derive the variational form of the sensitivity equation by differentiating (10) with respect to $\theta$. One seeks a $w_L(s) \in V = \{\varphi(\cdot) \in E\} \subset E = H^2(0,\ell/2)$ such that for all $\varphi \in V$

$$\begin{aligned} &\int_0^{\ell/2} \rho a \ddot{s}_{w_L}(t,s)\varphi(s)\ ds + \int_0^{\ell/2} EIs''''_{w_L}(t,s)\varphi(s)\ ds + \\ &\int_0^{\ell/2} \gamma_1 \dot{s}_{w_L}(t,s)\varphi(s)\ ds + \int_0^{\ell/2} \gamma_2 I \dot{s}''''_{w_L}(t,s)\varphi(s)\ ds \\ &= \int_0^{\ell/2} \frac{d}{dw}\left(\frac{-\Delta\text{Lift}(t,s)}{\ell/2}\right) s_{w_L}(t,s)\varphi(s)\ ds + \\ &\int_0^{\ell/2} b_L(s)\varphi(s)s_{u_L}(t)\ ds. \end{aligned} \tag{20}$$

Choose the same basis $\{b_i\}_{i=1}^N$ for the approximating space $V^N \subseteq V$ as was used in the state approximation. Then the state sensitivity is approximated as

$$s_{w_L}(t,s;\theta) \approx s_{w_L}^N(t,s;\theta) = \sum_{i=1}^N s_{c_i}(t)b_i(s), \tag{21}$$

and a finite dimensional approximation of (20) can be rewritten as a matrix equation

$$M_0\ddot{s}_c(t) + D_0\dot{s}_c(t) + K_0 s_c(t) = F_1(c(t), s_c(t)) + B_0 s_u(t;\theta), \tag{22}$$

where $s_c(t) = [s_{c1}(t), \ldots, s_{cN}(t)]^T$, $M_0$, $D_0$, $K_0$, and $B_0$ are defined in (18), and $F_1(c(t), s_c(t))$ is based upon the lift function. Convert (22) into a first order system by defining $s_{x1}(t) = s_c(t)$ and $s_{x2}(t) = \dot{s}_{x1}(t) = \dot{s}_c(t)$, thereby yielding

$$\begin{aligned} \begin{bmatrix} \dot{s}_{x1}(t) \\ \dot{s}_{x2}(t) \end{bmatrix} &= \begin{bmatrix} 0 & I \\ -M_0^{-1}K_0 & -M_0^{-1}D_0 \end{bmatrix} \begin{bmatrix} s_{x1}(t) \\ s_{x2}(t) \end{bmatrix} \\ &+ \begin{bmatrix} 0 \\ M_0^{-1}B_0 \end{bmatrix} s_{u_L}(t) + \begin{bmatrix} 0 \\ M_0^{-1}F_1(w_L(t), s_{w_L}(t)) \end{bmatrix}, \end{aligned} \tag{23}$$

where $s_x = [s_{x1}(t), s_{x2}(t)]^T = \left[s_{x1}(t), \frac{d}{dt}s_{x1}(t)\right]^T$. Combining (19) and (23) yields the coupled system

$$\begin{aligned} \begin{bmatrix} \dot{x}_1(t) \\ \dot{x}_2(t) \\ \dot{s}_{x1}(t) \\ \dot{s}_{x2}(t) \end{bmatrix} &= \begin{bmatrix} 0 & I & 0 & 0 \\ H_1 & H_2 & 0 & 0 \\ 0 & 0 & 0 & I \\ 0 & 0 & H_1 & H_2 \end{bmatrix} \begin{bmatrix} x_1(t) \\ x_2(t) \\ s_{x1}(t) \\ s_{x2}(t) \end{bmatrix} \\ &+ \begin{bmatrix} 0 \\ H_3\ u(t) \\ 0 \\ H_3\ s_u(t) \end{bmatrix} + \begin{bmatrix} 0 \\ H_4 \\ 0 \\ H_5 \end{bmatrix}, \end{aligned} \tag{24}$$

where $I$ is the identity operator and

$$\begin{aligned} &H_1 = -M_0^{-1}K_0,\ H_2 = -M_0^{-1}D_0,\ H_3 = M_0^{-1}B_0 \\ &H_4 = M_0^{-1}F_0(w(t)),\ H_5 = M_0^{-1}F_1(w(t), s_w(t)). \end{aligned} \tag{25}$$

Now, (24) is a finite-dimensional approximation to a system similar to the form of (1), where the additional terms appear due to the coupled sensitivity equation. One can replace the control $u_L(t)$ in (24) by the full state feedback control law

$$u_L(t;\theta) = -\mathscr{K}x(t;\theta) = -\mathscr{K}\begin{bmatrix} x_1(t) & x_2(t) \end{bmatrix}^T. \tag{26}$$

Furthermore, one can differentiate (26) with respect to $\theta$ to compute $s_{u_L}(t;\theta)$ as follows

$$\begin{aligned} s_{u_L}(t;\theta) &= \frac{d}{d\theta}u_L(t;\theta) \\ &= -R^{-1}\mathscr{B}^*\Pi\frac{dx(t;\theta)}{d\theta} - R^{-1}\mathscr{B}^*\frac{d\Pi}{d\theta}x(t;\theta) \\ &= -\mathscr{K}s_{w_L}(t;\theta) - R^{-1}\mathscr{B}^*\frac{d\Pi}{d\theta}w_L(t;\theta), \end{aligned} \tag{27}$$

where the sensitivity of $\Pi$ with respect to $\theta$, $\frac{d\Pi}{d\theta}$, is computed by differentiating (4) with respect to $\theta$ and solving a resulting Lyapunov equation [18], [19].

## IV. NUMERICAL RESULTS

To obtain a solution to the system in (24), initial conditions are chosen of the form: $x_1(0) = \sin\left(\frac{\pi s}{\ell}\right)$, $x_2(0) = \frac{\pi}{\ell}\cos\left(\frac{\pi s}{\ell}\right)$, $s_{x1}(0) = 0.75 * x_1(0)$, and $s_{x2}(0) = 0.75 * x_2(0)$. That is, to generate a nonzero state sensitivity, the authors choose the initial conditions for the sensitivity equation to be 75% of the initial conditions for the state equation. A finite element approximation using Hermite interpolating cubic splines of order $N = 20$ for the spatial discretization of *each* beam is employed to simulate (24), and the parameter values for the BMB system are as follows: $\ell = 10$ m, $\rho = 5.24$ kg/m$^3$, $\hat{w}$ (width) $= 1/\sqrt{48}$ m, $h$ (height) $= 1/\sqrt{48}$ m, $a = \hat{w}h = 1/48$ m$^2$, $E = 1.44 \times 10^9$ N/m$^2$, $I = 1/1327104$ m$^2$, $m = 5$ kg, $\gamma_1 = 0.025$ kg/(m s), $\gamma_2 = 1 \times 10^4$ kg/(m$^5$ sec). Originally, standard 4 degree of freedom beam elements were selected

for the finite element approximation, where the degrees of freedom correspond to displacements and slopes at the endpoints of each beam element (see for example [20]). However, due to numerical instabilities in solving the finite dimensional approximations to (4) and (5) with the 4 degree of freedom scheme, an approximation using 2 degrees of freedom, displacements at the end of each beam element, was developed. Numerical results from this approximation scheme are presented in this paper.

For this discretization and set of parameter values, it was found that the largest possible $H_\infty$ controller parameter $\theta$ that will guarantee $(I-\theta^2 P\Pi)$ being positive definite is 0.38. Therefore, all $H_\infty$ controllers implemented in this paper use $\theta = 0.38$. Still, the reader is reminded of the interest in examining the sensitivity of the state with respect to $\theta$ variation. In this work, the lift function is neglected, but it is included in the written statement of the model and relevant weak formulations since, ultimately, it is the intent that the BMB system will closely model a MAAS system.

Approximate state and state sensitivities to $\theta$ are computed for several values of the parameter, namely $\theta = 0.00$ (LQG compensator), $\theta = 0.10$, $\theta = 0.20$, and $\theta = 0.38$. For reference, the uncontrolled state plot is given in Figure 2. It is the intent to design a feedback controller that will stabilize the unstable uncontrolled system. The primary question of interest in this paper is how to take advantage of the aeroelastic wing feature of a MAAS to aid in control design efforts. A secondary goal is to examine how sensitive the controlled beam displacements are to variation in the $H_\infty$ control parameter, $\theta$. Figure 3 contains plots of the state sensitivities to the $\theta$ parameter. As can be seen from these simulations, the state sensitivities for the various $\theta$ values depicted are virtually indistinguishable. This observation suggests that for the BMB system with the chosen parameters, the actual $\theta$ value used in control design may not be critical in regard to controlled state performance.

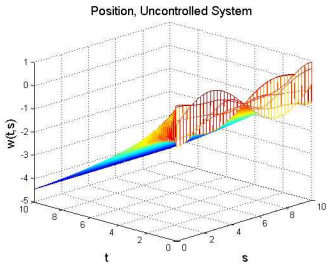


Fig. 2. Uncontrolled Position State

Additionally, the authors examine $s_u(t;\theta)$, the sensitivity of the controller with respect to $\theta$, and these plots are found in Figure 4. The results demonstrate that the controller becomes more sensitive to $\theta$ as this parameter is increased. Since the value of $\theta$ is closely connected to the robustness of the controller, this observation suggests that the more robust the controller, the more sensitive it is to $\theta$.

As a means to gain insight into the problem of sensor placement, the authors examine the control and observer

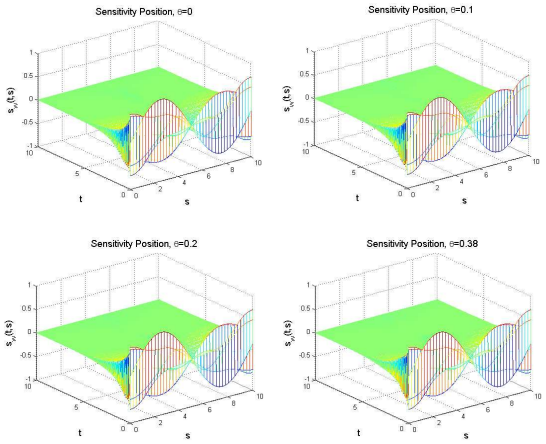


Fig. 3. State Sensitivities: $\theta = 0.00$ (top left), $\theta = 0.10$ (top right), $\theta = 0.20$ (bottom left), $\theta = 0.38$ (bottom right)

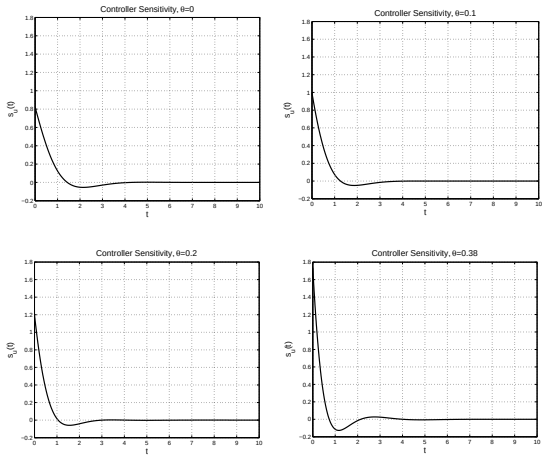


Fig. 4. Controller Sensitivities: $\theta = 0.00$ (top left), $\theta = 0.10$ (top right), $\theta = 0.20$ (bottom left), $\theta = 0.38$ (bottom right)

functional gains, contained in Figures 5 and 6, respectively. An area where a functional gain is large indicates that one should consider placing a sensor in that region of the spatial domain since it appears to contribute significantly to the control design. Due to the small scale of the control bending gains in Figure 5, there is no useful information to ascertain from this plot. The control velocity gains suggest that sensors be placed at the free ends of the beams. The observer gains in Figure 6 are nearly constant so that there is no useful information to ascertain from this plot. It should be noted that there may be a problem with convergence of the functional gains, as can be seen from the plots. Normally, one examines the functional gains for various discretizations with increasing $N$ to verify that gain convergence has been achieved. However, for $N = 5$ and $N = 10$ for each beam, MATLAB® reported that the Grammian matrix $W = [K_0\ 0; 0\ M_0]$ was nearly singular so that computation of $W^{-1}$, as required for gain computation (see [13]), may not be accurate. For this reason, and the fact that finer discretizations than $N = 40$ on each beam are computationally intractable due to

the cubic spline basis required for Euler-Bernoulli beam approximations, only gain computations for $N = 20$ and $N = 40$ for each beam are shown.

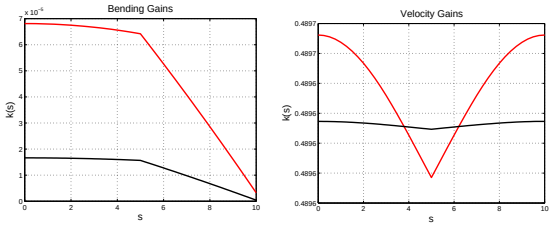


Fig. 5. Control Functional Gains for $\theta = 0.38$ with $N = 20$ (red) and $N = 40$ (black) for each beam: bending gains (left) and velocity gains (right)

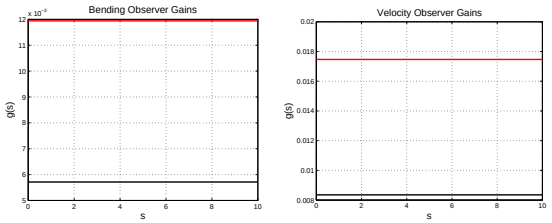


Fig. 6. Observer Functional Gains for $\theta = 0.38$ with $N = 20$ (red) and $N = 40$ (black) for each beam: bending gains (left) and velocity gains (right)

## V. CONCLUSIONS AND FUTURE WORKS

### A. Conclusions

In the paper, the BMB system (10), (11) is approximated by Hermite interpolating cubic splines with 2 displacement degrees of freedom for each beam element. Approximate state and state sensitivities to $\theta$ are computed for several values of the parameter $\theta$. It is observed that the state sensitivities for the various $\theta$ values depicted are virtually indistinguishable. This suggests that for the BMB system with the chosen parameters, the actual $\theta$ value used in control design may not be critical in regard to controlled state performance. The authors also examine the sensitivity of the controller with respect to $\theta$, and these results suggest that the more robust the controller, the more sensitive it is to $\theta$. As a means to gain insight into the problem of sensor placement, the authors examine the control and observer functional gains. The results suggest that placing sensors near the endpoints of the free ends of the beams may prove advantageous to control design.

### B. Future Works

Numerical instabilities in solving the finite dimensional approximations to the algebraic Riccati equations were discovered, and this needs to be investigated. More investigation needs to be done on the sensor placement problem in order to take into account sensor placement effects on performance and robustness. Instead of considering a point load between the two beams, the authors are interested in including in the BMB model a mass of some nonzero size. The authors plan to include a realistic aerodynamic force for the lift function.

## VI. ACKNOWLEDGMENTS

The authors gratefully acknowledge the contribution of the Louisiana Board of Regents, the US Air Force Summer Faculty Fellowship Program, the Air Force Research Laboratory and reviewers' comments.

## REFERENCES

[1] X. Tian, J. Iriarte-Diaz, K. Middleton, R. Galvao, E. Israeli, A. Roemer, A. Sullivan, A. Song, S. Swartz, and K. Breuer, "Direct measurements of the kinematics and dynamics of bat flight," *Bioinspiration & Biomimetics*, vol. 1, pp. S10–S18, 2006.

[2] A. Song, X. Tian, E. Israeli, R. Galvao, K. Bishop, S. Swartz, and K. Breuer, "Aeromechanics of membrane wings, with implications for animal flight," *AIAA Journal*, vol. 46, no. 8, pp. 2096–2196, 2008.

[3] W. Shyy, P. Ifju, and D. Viieru, "Membrane wing-based micro air vehicles," *Applied Mechanics Reviews*, vol. 58, pp. 283–301, 2005.

[4] W. Shyy, P. Trizila, C. Kang, and H. Aono, "Can tip vortices enhance lift of a flapping wing?" *AIAA Journal*, vol. 47, pp. 289–293, 2009.

[5] A. Chakravarthy, R. Albertani, N. Gans, and J. Evers, "Experimental kinematics and dynamics of butterflies in natural flight," *47th AIAA Aerospace Sciences Meeting Including The New Horizons Forum and Aerospace Exposition*, pp. AIAA–2009–873, 2009.

[6] R. Albertani, R. DeLoach, B. Stanford, J. Hubner, and P. Ifju, "Wind tunnel testing and nonlinear modeling applied to powered micro air vehicles with flexible wings," *AIAA Journal of Aircraft*, vol. 45, no. 3, 2008.

[7] A. Vargas, R. Mittal, and H. Dong, "A computational study of the aerodynamic performance of a dragonfly wing section ingliding flight," *Bioinspiration & Biomimetics*, 2008.

[8] L. Zheng, X. Wang, A. Khan, R. Vallance, R. Mittal, and T. Hedrick, "A combined experimental-numerical study of the role of wing flexibility in insect flight," *47th AIAA Aerospace Sciences Meeting Including The New Horizons Forum and Aerospace Exposition*, pp. AIAA–2009–382, 2009.

[9] R. Krashanitsa, D. Silin, S. Shkarayev, and G. Abate, "Flight dynamics of a flapping-wing air vehicle," *International Journal of Micro Air Vehicles*, vol. 1, pp. 35–49, 2009.

[10] B. M. Chen, "Non-iterative computation of optimal value in $h_\infty$ control," in *Unsolved Problems in Mathematical Systems and Control Theory*, V. D. Blondel and A. Megretski, Eds., Princeton: Princeton University Press, 2004, pp. 271–275.

[11] J. C. Doyle, K. Glover, P. P. Khargonekar, and B. A. Francis, "State-space solutions to standard $h_2$ and $h_\infty$ control problems," *IEEE Transactions on Automatic Control*, vol. 34, no. 8, pp. 831–847, 1989.

[12] I. Rhee and J. Speyer, "A game theoretic controller and its relationship to $h_\infty$ and linear-exponential-gaussian synthesis," *Proceedings of the 28th Conference on Decision and Control*, pp. 909–915, 1989.

[13] J. S. Gibson and A. Adamian, "Approximation theory for linear quadratic gaussian control of flexible structures," *SIAM J. Contr. Opt.*, vol. 29, pp. 1–37, 1991.

[14] J. A. Burns and B. B. King, "A reduced basis approach to the design of low order feedback controllers for nonlinear continuous systems," *Journal of Vibration and Control*, vol. 4, pp. 297–323, 1998.

[15] J. A. Atwell and B. B. King, "Reduced order controllers for spatially distributed systems via proper orthogonal decomposition," *SIAM J. Sci. Comput.*, vol. 24, no. 1, pp. 128–151 (electronic), 2004.

[16] A. L. Faulds and B. B. King, "Centroidal voronoi tesselations for sensor placement," *Proc. IEEE CCA/CACSD 2000, Anchorage AK*, pp. 536–541, 2000.

[17] B. B. King, "Nonuniform grids for reduced basis design of low order feedback controllers for nonlinear continuous systems." *Mathematical Models and Methods in Applied Sciences*, vol. 8, no. 7, pp. 1223–1241, 1998.

[18] J. T. Borggaard and J. Vance, "Sensitivity equations for the design of control systems," *Proceedings of Control and Applications*, 2004.

[19] L. Zietsman, K. A. Evans, J. T. Brown, and R. A. Idowu, "Riccati conditioning and sensitivity for a minmax controlled cable-mass system," *Proceedings of IEEE Conference on Decision and Control*, 2008.

[20] C. Desai and T. Kundu, *Introductory Finite Element Method*. Boca Raton, Florida: CRC Press LLC.

# Issues of Scale in Agile Micro Autonomous Systems

Johnny H. Evers[1]
*Air Force Research Lab, Munitions Directorate, Eglin AFB, FL 32542*

**The quest for micro autonomous systems (MAS) is taking us from the realms of science and engineering, as with the University of California at Berkeley micro mechanical flying insect, to areas that would have been the realm of science fiction just a few years ago, as in Darpa's Nano Air Vehicle program. Emboldened by advances in micro-scale technologies and inspired by insight into the mechanisms associated with biological locomotion, eventual realization of bird or insect size autonomous robots seems certain. Among the many technical challenges, issues associated with integration of MAS into complex human-directed information networks, in particular issues of autonomous sensory-response architectures for systems with multi-scale dynamics, may prove to be the largest hurdles. This paper speculates on the existence of a fundamental characteristic of autonomous systems that may underlie those hurdles.**

## I. Introduction

HUMAN engineered systems increasingly rely on automation to enhance performance, provide fault tolerance and allow the operator to concentrate on high-level decisions as opposed to low-level motor control tasks. These systems are designed to be responsive to human-generated commands but at the same time robust to disturbances that may require corrections several orders of magnitude faster than human response times. Advanced fighter aircraft, for example, maneuver at the edge of human sensory-response capabilities by having autopilots that stabilize the aircraft through operating regimes beyond the capabilities of direct human control. Artificial limits on the aircraft operational envelope, which are imposed on the aircraft performance to accommodate the limitations of human physiology and sensory-response capabilities, are made necessary by the critical role of the human as pilot of the vehicle. In effect, the human operated fighter aircraft has an outer-loop/inner-loop flight control system in which the pilot provides the sensing, decision processing and command functions to the inner-loop autopilot which, in turn, stabilizes the aircraft flight during maneuvers. This time- or frequency-based separation into a relatively high-bandwidth inner stabilization loop and a lower-bandwidth outer command loop is a common control system architecture that requires the physical response of the vehicle in its interactions with its surroundings to be separable into fast and slow dynamics. While this separation is usual and physically justified in manned aircraft and large UAVs, it may not be applicable to agile MAS capable of aggressive maneuvers in confined space where the relative kinematics between a MAS and other nearby objects may require a response bandwidth on the same time scale as the MAS body rotational dynamics. Imposing the usual separation of slow and fast dynamics on a MAS design, for example by reducing its response bandwidth to mitigate coupling with its body dynamics, will result in stable but sluggish vehicles that have only limited agility.

Of course, the vision is for MAS to achieve or even exceed the agility, performance and robustness of living systems. We entertain notions of small groups of MAS capable of flight through urban centers much like flocks of ubiquitous pigeons (Figure 1). These flocks of engineered vehicles would have the flight capabilities of flying animals but will be under the overall supervision of one or more human operators. That is, the MAS would require significant autonomous flight capabilities to negotiate the confined and high uncertainty environment while requiring positive human control of the vehicle swarm. Putting aside the various ethical issues of associated with use of autonomous vehicles in human-occupied environments, the challenges imposed by the multi-scale dynamics inherent in this scenario are large. Human command and decision processes may span minutes to days, while the dynamics associated with micro-scale flight may evolve over milliseconds. Errors at the human decision level have obvious potential to impact the overall system performance, from failure to perceive and act upon a critical piece of information to issuing erroneous commands. Similarly, errors at the MAS level propagate upward to the human decision level, producing gaps in critical information or distorting the context of otherwise correct information. The

[1] AFRL/RWAV, 101 W. Eglin Blvd, Ste 332, Associate Fellow AIAA

emergent consequences of these different scales of errors are impossible to predict with our current system modeling tools. Thus, consequences of a MAS's erroneous positive response to a benign chemical signature may be negligible, merely resulting in the vehicle flying into a nearby window and disrupting a peaceful family dinner. Alternatively the consequences may be tragic, prompting escalation of a minor into a major disaster. Unfortunately, our capabilities of engineering MAS seem to be outpacing our understanding of how to incorporate them into fault resistant human decision networks.

**Figure 1. Group of agile MAS entering an urban canyon**

This paper takes the perspective that agile MAS with their layers of human supervision represent complex, highly nonlinear multi-scale dynamical systems. After a brief discussion of some issues of scale for such systems and current research investigating those issues, the paper will focus on the idea of autonomy associated with multi-scale dynamical systems. Agile MAS currently exist only in nature (i.e., insects, birds, bats). Consequently, the paper will consider autonomy in manmade MAS from a biological perspective. That is, it will speculate that functional system characteristics associated with the capabilities of living flying organisms may require levels of response variation and flexibility that are not associated with, and perhaps will not be tolerated in manmade critical systems. Although this paper will not directly address questions of ethics associated with the deployment of critical autonomous systems, it will attempt to provide some insight into how those important questions may naturally emerge when any degree of robustness is imposed as a design criterion for manmade agile autonomous systems.

## II. Automatic Control

For present purposes, 'dynamical systems' can be thought of as systems which evolve through time. Mathematically their behavior can be described by combinations of differential or difference equations. In addition to familiar examples such as objects in motion, fluid flow and heat flow, this definition also covers modern 'information networks' such as human decision systems, the internet, networked communication systems, and command & control systems.

Dynamical systems which evolve over a narrow time scale range can be characterized using a rich body of descriptive and computational mathematics. An automobile operating on cruise control provides a familiar example. A complete description of all of the dynamics associated with engine, friction and aerodynamic forces is of extremely high order. It involves time scales ranging from those of the combustion processes, motion induced aerodynamic turbulence and heat flux during severe braking to those of the vehicle accelerator response, certainly several orders of magnitude. While on cruise control however, the vehicle accelerates or decelerates in response to road grade or wind variations to maintain a relatively constant speed. In this cruise mode, the dominant dynamics associated with the vehicle motion are adequately described as a compact set of 3 linear $1^{st}$ order differential equations with a time constant on the order of seconds. Actually most familiar manmade systems, whether home heating/cooling systems, home power generators or automatically piloted commercial aircraft are designed to exhibit this sort of relatively linear, narrow bandwidth response.

Some manmade systems do not lend themselves to such a compact mathematical description. The most agile air vehicles currently produced, tactical air intercept homing missiles, provide an interesting example of a wide-scale dynamical system. A reasonably minimal description of such a missile during the later phases of a target engagement would be of relatively high order and highly nonlinear. These dynamics would include the target detection and warhead event, associated with fractions of millisecond time constants; the vehicle rigid body dynamics, having 10s of millisecond time constants; and the intercept kinematics, having 100s of millisecond time constants. As is typical for such systems, during the design process these different time scale dynamics are treated separately. The warhead and target detection system are designed separately from the missile autopilot; the autopilot is designed to stabilize the body rotational dynamics and to achieve the guidance system commanded accelerations; and the guidance system is designed generate acceleration commands to steer the missile close to an intercept with the target.[1]

Continuing with this example, a missile developed to intercept high agility targets requires guidance systems capable of high bandwidth response (i.e., small time constants). This, in turn, requires that the autopilot have a much higher bandwidth response, typically with 0.2 or smaller time constants than that of the guidance system. Of course the airframe itself must be capable of achieving such small response time constants. For example, consider how fast you can move a long flexible fishing rod versus a short stiff one. Move the long flexible rod relatively slowly and the rod tip will follow the hand motion. Move it more quickly and the tip motion will be out of phase with the hand motion. The short stiff rod, however, may be moved as quickly as you can with minimal deflection. Likewise, the missile airframe must be stiff enough to produce the accelerations required to intercept the target. The design of a wide bandwidth system such this challenges the capabilities of the tools of automatic control.[2]

Automatically controlled dynamical systems have become pervasive in our technology-based society. From climate control systems in homes and buildings to automated aircraft landing systems, the notion of manmade systems responding to changing conditions on their own has become a familiar one. The idea of sensing some error in desired response and generating a correction proportional to that error is intuitive and has its origin in antiquity. A textbook example is that of the mechanical governor of James Watt's steam engine. As engine speed increases/decreases, a spinning pendulum device decreases/increases steam to the engine through a mechanical linkage. This allows the engine to respond to varying loads with consistent performance without operator intervention, a measure of system 'performance', and prevents the engine from exceeding its cycling limits if the load is abruptly changed, a measure of system 'robustness'. The rate at which the speed of the governed engine can accommodate load variations is a measure of its response bandwidth. Again, it is intuitive that beyond a threshold rate, very rapid changes to the engine load will exceed the response capabilities of the engine system. For example, this limited response may result from a response latency or time delay in steam flow to increase in engine speed. These characteristics of performance, robustness, bandwidth, and time delay sensitivity comprise some of the principle figures of merit for any controlled dynamical system. This example also illustrates another key feature of most automatically controlled dynamical systems: that the operator interacts with the system through modulation of the controller. That is, the engine speed is regulated by adjusting the governor rather than directly adjusting the steam flow. Thus, the human operator can be thought of as an 'outer loop controller', modifying the speed range of the engine based on his own sensing processes, with the actual speed of the engine regulated by the 'inner loop controller', the governor/steam regulator.

Manmade automatically controlled machines are usually designed to provide a fairly linear response to commands, however nonlinear the underlying dynamics may be. In effect, the controller cancels the undesirable dynamics and replaces them with a desired linear dynamical response. Image stabilization in modern digital point and shoot cameras provides a rather familiar example of this cancellation of dynamics. Photographer motion is sensed and compensated through any of various mechanisms so that much of the motion-induced blur is removed from the resulting image. Any photographer motion beyond the bandwidth of the image stabilization system will appear as image blur.

In the early half of the 20$^{th}$ century, mathematicians such as Norbert Wiener and colleagues established information and decision theory as a foundation for development of dynamics and control systems theory and methodology.[3] Beginning with rudimentary notions of feedback (e.g., the modulation of dynamics based on sensed signals in Gibb's mechanical governor) the latter half of the 20$^{th}$ century saw the birth and maturation of theories of linear multivariable, linear robust, stochastic linear, adaptive, nonlinear, distributed parameter and cooperative control, to name only a few categories. Based on the mathematics of linear algebra, set theory, real and complex analysis, optimization and so on, the methodologies and tools available for control system design have become essential to the operation of many engineered systems from compact disc players to commercial aircraft.[4]

These tools are not without their limitations. To continue the example of a tactical air intercept missile, separation of the control design into an inner autopilot stabilization loop and an outer guidance intercept loop

imposes an artificial limitation on the missile intercept performance. With a high order dynamics description of the coupled intercept kinematics and vehicle body dynamics of sufficient fidelity, a designer can produce a very high-bandwidth controller that directly computes missile fin deflection commands from measurements of target maneuver. Unfortunately, such a controller is very brittle in the sense that its response degrades or even becomes unstable in the presence of inevitable errors in the dynamics model, unmodeled time delay, unmodeled high-frequency dynamics, unpredictable disturbances, uncharacterized sensor noise, and target maneuver uncertainties. Throughout the 1990's, many publications described various attempts to design integrated guidance and control systems that recovered some of the response bandwidth sacrificed with inner-outer-loop designs. Few of these approaches have been successful in practice for reasons of high design cost (e.g., requiring high-bandwidth actuators, extensive tests to produce accurate dynamics models, low noise sensors, low airframe manufacturing tolerances, etc.) and lack of real-world robustness, the latter due to a combination of control methodology limitations and the realities of operation in stressing environments.[5]

Much of the research on integrated guidance and control, and wide-bandwidth control in general, focuses on increasing performance rather than robustness. The field of adaptive control instead focuses on increased robustness, or equivalently expansion of the performance regime of the system. Adaptive controllers implicitly or explicitly learn the unmodeled or unknown system dynamics and modify the control signal to accommodate their impact on the desired system response. Early adaptive control methods simply adjusted the controller gain to zero the error between desired and actual system output responses. More recent adaptive control schemes inject an additional control signal to preserve a system's nominal response in the face of uncertainty or disturbances. Some of the most interesting and useful advances in control theory have occurred in adaptive control theory in the past ten-fifteen years. Although useful in process control applications such as chemical processing and plants, the aerospace industry has been slow to accept adaptive control. In the past decade however, newer methods for design of adaptive controllers have been applied to manned experimental aircraft and precision guided bombs.[6,7]

While manmade automatic control systems are common, manmade autonomous systems are not. The reasons for this require some explanation of the differences between the two concepts. Essentially all automatic control systems are designed to produce desired response in operation over rather narrow operating regimes. This may be accomplished through a combination of limiting the response bandwidth (i.e., essentially the closed loop systems ignores disturbances, inputs and noise beyond its response bandwidth) and *ad hoc* limits imposed on the system response (e.g., min/max thermostat temperatures, RPM limiters on motor control systems, physical stops on actuators, cut-out switches, etc.). These features allow the automatic control system to operate without human intervention for long periods, delivering predictable response in the face of outside disturbances; the automobile cruise control comes to mind.

In casual usage, autonomy implies a level of response robustness beyond that associated with more familiar automatic control systems, whether adaptive or not. For example, a commercial aircraft autopilot allows steady cruise, climb or descent in the presence of varying winds, but an autonomous landing system must allow the aircraft to negotiate the far more uncertain wind conditions near the ground. Note, however that these kinds of 'autonomous' systems are still designed for very predictable response in the presence of an expanded range of uncertain, but reasonably characterizable dynamic disturbance conditions. For present purposes, these kinds of systems will be considered an elaboration of automatic control systems.

The concept of autonomy as used in this paper is illustrated by examples from the science fiction genre of motion pictures: the spacecraft computer Hal in the movie *2001: A Space Odyssey*, the cyber organisms in the *Terminator* movies, or the robot Sonny in the movie *I Robot*. These fictitious robots demonstrate both high levels of response robustness and similarly high levels of flexibility in response. That is, they vary their responses to be appropriate to the context of the current and anticipated situations in ways that seem very 'life-like'. These are systems that can be given a mission and allowed to respond as they will during the course of accomplishing the mission. This is a very different sort of behavior from that of an automatic control system, whether adaptive or not. And it is specifically this kind of behavior that is implied, whether intentionally or not, by many descriptions of MAS.[8]

To be a bit more specific, this concept of autonomy implies flexible and context-appropriate behavioral response in the presence of real world unpredictable external events. Imagine a cooperative group of MAS flying through an urban canyon searching for a particular vehicle. These vehicles presumably have the sensory capability necessary to detect, identify and track the truck as well as to avoid collision with buildings, signs, power lines and each other. Similarly, they presumably have sufficient aerodynamic agility to chase the truck, once it is identified, through the congested streets while maneuvering to avoid collisions and to coordinate their efforts. And these sensory response capabilities are robust to the high uncertainties associated with urban canyons: wide variations in

ambient luminance; surface textures varying from concrete to painted or reflective surfaces; as complex an acoustic environment as may be imagined; wind gusts that may exceed the vehicle flight speed; etc.[9]

The concluding sections of this paper suggest that the behavior of autonomous mobile systems involves variation and flexibility in response that is significantly different from that of manmade automatic control systems, whether adaptive or not. And the basis for this point of view begins with the observation that the capabilities required for this urban canyon MAS scenario are 'life-like', in the sense of that imagined by writers of the movies mentioned above.

## III. Agility and Autonomy in Biological Flight

Although the notion of automatic operation was a rare feature of human technology until the last century, and the notion of autonomy as described in the previous section is essentially absent from current human engineered mobile systems, autonomy is an inherent feature of biological systems response at all size and temporal scales. Somewhat surprisingly, this is an underappreciated fact given the incredible diversity of life processes and life forms on the Earth. In order to see this, the response of manmade automatic control systems needs to be contrasted with that of biological processes.

Return to the example of a tactical air intercept missile once again. The missile autopilot is designed to reject disturbances and produce airframe acceleration response to guidance commands over a range of altitude and velocity conditions that comprise the operational envelope for the missile. Within limits imposed by the autopilot design or control surface effectiveness, the autopilot will track whatever commands the guidance law generates and do so with a certain error and latency. Analogously, think of using the cruise control to modulate speed to accommodate the flow of traffic on an interstate highway. At first glance, this would seem to be similar to the response associated with a Peregrine falcon steady flight, perhaps with other hawks, during a seasonal migration.

The missile guidance system, itself an outer-loop feedback control system for the closed-loop autopilot controlled airframe dynamics, estimates the relative motion of the target with respect to the missile and generates acceleration commands to maintain an intercept course with the target. As the target maneuvers, the acceleration commands to the autopilot are automatically adjusted so that the missile maneuvers to accommodate target motion. As long as the acceleration commands do not exceed the autopilot magnitude limits, and the guidance system bandwidth is sufficiently low with respect to the autopilot/airframe bandwidth, the autopilot will track the commands and the missile will intercept the target within a certain margin of error. Further, the missile guidance system can be expected to have been designed in such a way that it will try to maintain an intercept course to the target in spite of target attempts to flee or to deceive the missile guidance system. Again, this would seem to be very similar to a Peregrine falcon's predation attempts on a fleeing duck or grouse.

The predicted performance of a tactical air intercept missile is often characterized by mean and standard deviation of the distance of closest approach in Monte Carlo simulation analysis. Reasonable random and bias errors, various target maneuvers, and various engagement initial conditions are introduced into a high fidelity dynamics simulation of the intercept scenario to account for the dominant uncertainties inherent real world scenarios. The missile system designer tries to adjust the various design parameters at his/her disposal to minimize expected miss distance (in the sense of mean and variance as measured through the Monte Carlo analysis) over all expected engagement conditions. Over the lifespan of the missile type, the design may be further refined based on analysis of flight tests or real world engagements. In any event, the design objective can be summed up as producing a *desired nominal behavior* characterized by minimized mean and variance of miss distance (or other suitable figure of merit). Further, the design analysis may establish confidence intervals associated with the nominal behavior, a measure of system robustness. While the details may differ greatly among other human engineered mobile automatic control systems, the design objective of *desired nominal behavior* over some range of conditions (i.e., robust) seems to be nearly universal.

A perusal of the animal behavior literature at first seems very familiar in the context of the discussion of the preceding paragraphs. Biologists make observations of animal responses, whether to artificial stimuli in a laboratory experiment or to natural stimuli in the field, characterize the responses using metrics such as mean and standard deviation, and establish confidence intervals using various statistical tests. Especially within many biology experimental laboratories, there seems to be an almost engineering mindset to describe *nominal behavior* and characterize variations with respect to the nominal. This is only good science! Experiments are carefully designed to be replicated a sufficient number of times so that statistical analysis of the results will be valid, allowing readers of the published results to infer the relative merits of the conclusions. Plots of response often include error statistics that may suggest, especially to the non-biologist, an almost engineered *nominal response*. This seems to be true whether the experiments involve study of behavioral intraspecific interactions among animals; study of the neurobiology of animal sensory systems; reconstruction of flight mechanics and aerodynamics of animals flying in

wind tunnels; response of physiological processes to perturbations; study of biochemistry associated with metabolic processes; study of cellular mass and energy transport mechanisms; or study of protein transcription or nucleic acid replication.

The complexity of biological system responses at all scales requires this kind of approach. In order for an experiment or study to be capable of being replicated, which is an obvious requirement of a credible scientific endeavor, experimental conditions must be controlled, or the observational study scope narrowly defined, so that response and stimuli may be reliably correlated. While this is true with the study of any complex phenomenon, it seems to be inherent in essentially every biological study.

Unfortunately, and this is speculation, it seems that these tendencies to *nominal behaviors* exist primarily over conditions associated with the specific study. An impression one gathers from discussions with biologists or from the published literature is that variation in response among different individuals within the same species, or even among subsequent trials with the same individual test subject, is large. Furthermore, this response variation may be correlated with very subtle differences among conditions in subsequent experimental setups; differences that would seem to be irrelevant in the context of the study.

Similar impressions arise almost immediately from reading studies of animal social behavior. In vertebrate observational studies, behavioral differences among individuals in a social group often allow researchers to distinguish individuals at a glance. Read Jane Goodall's accounts of the Gombe Reserve chimpanzees or George Schaller's studies of lion prides on the Serengeti.[10,11] But this also seems to hold to a significant degree for fish schools, passerine bird flocks, bat colonies, in fact for any vertebrate group you can think of. Not only do animals assume different roles within structured social groups, but the behaviors of different animals playing the same roles differ in significant ways. The layperson impression of homogeneity in response for these organisms may only be due to limited resolution of the observation (e.g., sheep, and their shepherds, recognize other sheep!).

Animals typically associated with more stereotyped behavior also seem to exhibit large individual variations in response. It has long been known that honeybees change behavioral roles within a colony as they age. Stress, variations in food supply, weather conditions and other external conditions can modify the timing of these maturation effects. And as with vertebrates, honeybees show individual behavioral differences even within the same age class. Again, discussion with insect biology experimentalists leaves one with the impression that insect behavior is far from being predictable to the degree that one associates with well-engineered mechanical systems.

## IV. Implications for Manmade Autonomous Systems

To set the stage for the closing discussion, consider the following behavioral study thought experiment. Choose at random 100 missiles of a given model and fire them one at a time against targets of a given type under a range of reasonable engagement conditions. Chances are very good that the distributions of miss distances, times to intercept, trajectories, etc., would be consistent with, though not identical to those obtained from a Monte Carlo simulation study of the same missile model evaluated over a similar range of scenarios. That this is a reasonable expectation emerges from two related phenomena: the dynamics models in the simulation have been refined to yield a high fidelity representation of the actual scenarios; and the missiles have been designed to yield consistent, reproducible *desired nominal behavior*. This kind of predictable behavior is often termed 'mechanistic', even when ascribed to human behavior such as that of a choreographed dance performance.

Now perform an analogous experiment with a falconer releasing 100 trained Peregrine falcons of similar age and training experience one at a time against a sequence of fleeing grouse (recall it is a thought experiment). On any given day, the flight performance of a trained bird-of-prey such as a falcon may be influenced by many factors including how recently it has eaten, its molt condition, the season, its general state of health, etc. Although these are trained animals, one would not be surprised to find the performance variation to be quite large. That is, the spreads in the distributions of number of passes to capture, times to capture, paths flown during the pursuit, etc. would be large when compared with related figures of merit in the missile experiment. We expect this since animals, after all, are animals and their behavior is rarely 'mechanistic' in the sense of being highly predictable over long time scales.

Finally perform a similar experiment with release of 100 wild, untrained Peregrine falcons, again of similar ages, one at a time against a sequence of fleeing grouse. We naturally expect the performance variation to be even larger than with the trained animals. The object of the training, after all, is to produce repeatable, predictable *desired nominal behavior*.

What does this have to do with design of agile MAS? Even if these observations with respect to biological autonomous response are valid as conjectured, correlation of response flexibility with autonomy does not imply causation. Biological systems that emerge through the interplay of the complex processes of evolution may exhibit response variation as a byproduct of the variations necessary for powering evolution. Certainly, species with highly specialized behavior are more seriously affected by environmental change than those with more varied behavioral

repertoires. Many of the animal extinctions of the past few centuries involve such ecological or behavioral specialists. Hence animals capable of tolerating large ecological perturbations would naturally be supposed to have behavioral repertoires, individually and/or collectively, that allow adaptation to the environmental fluctuations.

Although correlation certainly does not imply causation, an argument can be developed that suggests behavioral response flexibility is, in fact, naturally and intrinsically associated with autonomous behavior. Further, that MAS capable of interacting with their surroundings in the complex ways envisioned by technologists will, at the very least, exhibit the variations in response associated with highly trained animals (or human groups!) and will not exhibit the relative high performance predictability currently associated with automated machines. Anyone who has walked a normally well behaved male dog in the vicinity of a female dog in season will appreciate the difference.

An outline of such an argument might begin with consideration of *autonomous systems that exhibit context-appropriate behavioral responses to essentially unpredictable events*. One might then make the following assertions, each of which is disprovable, at least in principle:

- Real world complex environments, whether natural or manmade, generate unpredictable events over behaviorally relevant time and spatial scales
- It is impossible to model the important dynamics real world complex environments, whether natural or manmade, at sufficient levels of fidelity required to *a priori* define context-appropriate responses
- The degree of flexibility associated with a behavioral repertoire, independent of the size of a behavioral repertoire, determines the range of context-appropriate responses available
- The range of context-appropriate responses available determines the range of unpredictable events that can be accommodated

A reasonable inference from these assertions is that environmental complexity drives a requirement for behavioral response flexibility and makes it a necessary attribute for any system capable of accommodating uncertainties associated with a real world complex environment. This, of course, falls far short of a proof that behavioral response flexibility is necessarily associated with autonomous systems, but it motivates consideration of the possibility that such might be the case. The possibility merits further investigation.

If the preceding discussion has merit, the natural question emerges of whether human society is prepared to accept that MAS may operate more like trained animals than more familiar automated mechanical devices. We are reasonably comfortable with the knowledge that even highly domesticated animals occasionally exhibit undesirable behavior. Whether we can become comfortable with the potential for similar behavior from MAS will be an open question until such systems arrive.

## References


1. Zarchan, P., 2007, *Tactical and Strategic Missile Guidance*, AIAA series Progress in Astronautics and Aeronautics.
2. Blakelock, J.H., 1991, *Automatic Control of Aircraft and Missiles*, Wiley Interscience Publications.
3. Wiener, N., 1948, *Cybernetics: Or Control and Communication in the Animal and the Machine*, MIT Press, Cambridge Mass.
4. Kuo, B., 1982, *Automatic Control Systems*, Prentice Hall.
5. Cloutier, J.R., Evers, J.H., Feeley, J.J., 1988, "An Assessment of Air-to-Air Missile Guidance and Control Technology", Proc. American Control Conf..
6. Calise, A.J., Sharma, M., Corban, J.E., 2000, "Adaptive Autopilot Design for Guided Munitions", AIAA Journal of Guidance, Control and Dynamics, Vol 23., No 5.
7. Cao, C., Hovakimyan, N., Lavretsky, E., 2006, "Application of $L_1$ Adaptive Controller to Wing Rock", Proc. AIAA Guidance, Navigation and Control Conf.
8. Evers, J.H., 2007, "Biological Inspiration for Agile Autonomous Air Vehicles", NATO RTO AVT-146 Session on Platform Innovations and System Integration fro Unmanned Air, Land and Sea Vehicles.
9. Ol, M., Parker, G., Abate, G., Evers, J., 2008, "Flight Controls and Performance Challenges for MAVs in Complex Environments", Proc. AIAA Atmospheric Flight Mechanics Conference.
10. Goodall, J., 1996, *My Life with Chimpanzees*, Aladdin Press.
11. Schaller, G. B., 1976, *The Serengeti Lion: A Study of Predator-Prey Relations*, Univ. of Chicago Press.

DISTRIBUTION LIST
AFRL-RW-EG-TP-2011-006

Defense Technical Information Center — 1 Electronic Copy (1 File & 1 Format)
Attn: Acquisition (OCA)
8725 John J. Kingman Road, Ste 0944
Ft Belvoir, VA 22060-6218

---

EGLIN AFB OFFICES:

AFRL/RWOC (STINFO Office) - 1 Hard (Color) Copy
AFRL/RW CA-N - STINFO Officer Provides Notice of Publication

AFRL/RWG - 1 Copy
AFRL/RWM - 1 Copy
AFRL/RWP - 1 Copy